Article

Pattern-recognition receptors are required for NLR-mediated plant immunity

https://doi.org/10.1038/s41586-021-03316-6

Received: 14 April 2020

Accepted: 1 February 2021

Published online: 10 March 2021

Check for updates

Minhang Yuan[1,2], Zeyu Jiang[1,2,10], Guozhi Bi[3,4,10], Kinya Nomura[5,10], Menghui Liu[6], Yiping Wang[1], Boying Cai[1,2], Jian-Min Zhou[3,4], Sheng Yang He[5,7,8] & Xiu-Fang Xin[1,2,9]✉

The plant immune system is fundamental for plant survival in natural ecosystems and for productivity in crop fields. Substantial evidence supports the prevailing notion that plants possess a two-tiered innate immune system, called pattern-triggered immunity (PTI) and effector-triggered immunity (ETI). PTI is triggered by microbial patterns via cell surface-localized pattern-recognition receptors (PRRs), whereas ETI is activated by pathogen effector proteins via predominantly intracellularly localized receptors called nucleotide-binding, leucine-rich repeat receptors (NLRs)[1–4]. PTI and ETI are initiated by distinct activation mechanisms and involve different early signalling cascades[5,6]. Here we show that *Arabidopsis* PRR and PRR co-receptor mutants—*fls2 efr cerk1* and *bak1 bkk1 cerk1* triple mutants—are markedly impaired in ETI responses when challenged with incompatible *Pseudomonas syrinage* bacteria. We further show that the production of reactive oxygen species by the NADPH oxidase RBOHD is a critical early signalling event connecting PRR- and NLR-mediated immunity, and that the receptor-like cytoplasmic kinase BIK1 is necessary for full activation of RBOHD, gene expression and bacterial resistance during ETI. Moreover, NLR signalling rapidly augments the transcript and/or protein levels of key PTI components. Our study supports a revised model in which potentiation of PTI is an indispensable component of ETI during bacterial infection. This revised model conceptually unites two major immune signalling cascades in plants and mechanistically explains some of the long-observed similarities in downstream defence outputs between PTI and ETI.

PRRs are cell surface-localized receptor-like kinases and proteins (RLKs and RLPs) with an extracellular ligand-binding domain that senses conserved molecular patterns from diverse microorganisms. By contrast, NLRs are predominantly intracellular proteins that sense pathogen-derived effector proteins inside the plant cell and can be further classified into the coiled-coil (CC) type, the TOLL/INTERLEUKIN-1 RECEPTOR/RESISTANCE PROTEIN (TIR) type or the RPW8 (CC_R) type, depending on their N-terminal domain[7]. Signalling initiated by PRRs and NLRs leads to largely overlapping downstream cellular responses, including defence-gene expression, production of reactive oxygen species (ROS) and callose deposition[8,9], but the mechanism(s) by which this occurs and the nature of potential signal cooperation between cell surface and intracellular perception systems has remained unclear.

PRR and co-receptors are required for ETI

Using the *Arabidopsis thaliana–P. syringae* pathosystem, we uncovered an unexpected role of PRR and its co-receptors (hereafter PRR/co-receptors) in ETI. Specifically, an avirulent, ETI-eliciting bacterial strain, *P. syringae* pv. *tomato* (*Pst*) DC3000(*avrRpt2*), which activates RESISTANCE TO *P. SYRINGAE* 2 (RPS2)-dependent ETI in wild-type plants[10,11], did not elicit effective ETI in two separate PRR/co-receptor *Arabidopsis* mutants, *fls2 efr cerk1* (*fec*) and *bak1 bkk1 cerk1* (*bbc*), which lack major PRR/co-receptors that recognize bacteria-associated molecular patterns[12]. As shown in Extended Data Fig. 1a, the *fec* and *bbc* mutants did not mount an effective ETI response against *Pst* DC3000(*avrRpt2*). A similarly compromised ETI phenotype as in *fec* and *bbc* mutants was also observed with AvrPphB and AvrRps4, which are recognized by RPS5[13] and RPS4[14], respectively, in *Arabidopsis* Col-0 (Extended Data Fig. 1b), suggesting a potentially broad role of PRR/co-receptors in ETI. We subsequently focused on ETI triggered by the secreted bacterial effector protein AvrRpt2 (hereafter referred to as ETI) for in-depth characterization. Hypersensitive response, manifested by rapid cell death during ETI, was delayed in *fec* and *bbc* mutants in response to *Pst* DC3000(*avrRpt2*), as evidenced by less hypersensitive-response-associated leaf tissue collapse 7 h after bacterial infiltration (Extended Data Fig. 1c).

[1]National Key Laboratory of Plant Molecular Genetics, CAS Center for Excellence in Molecular Plant Sciences, Institute of Plant Physiology and Ecology, Chinese Academy of Sciences, Shanghai, China. [2]University of Chinese Academy of Sciences, Beijing, China. [3]State Key Laboratory of Plant Genomics, Institute of Genetics and Developmental Biology, Innovation Academy for Seed Design, Chinese Academy of Sciences, Beijing, China. [4]CAS Center for Excellence in Biotic Interactions, University of Chinese Academy of Sciences, Beijing, China. [5]Department of Energy Plant Research Laboratory, Michigan State University, East Lansing, MI, USA. [6]Key Laboratory of Plant Stress Biology, State Key Laboratory of Cotton Biology, School of Life Sciences, Henan University, Kaifeng, China. [7]Howard Hughes Medical Institute, Duke University, Durham, NC, USA. [8]Department of Biology, Duke University, Durham, NC, USA. [9]CAS-JIC Center of Excellence for Plant and Microbial Sciences (CEPAMS), Institute of Plant Physiology and Ecology, Chinese Academy of Sciences, Shanghai, China. [10]These authors contributed equally: Zeyu Jiang, Guozhi Bi, Kinya Nomura. ✉e-mail: xinxf@sippe.ac.cn

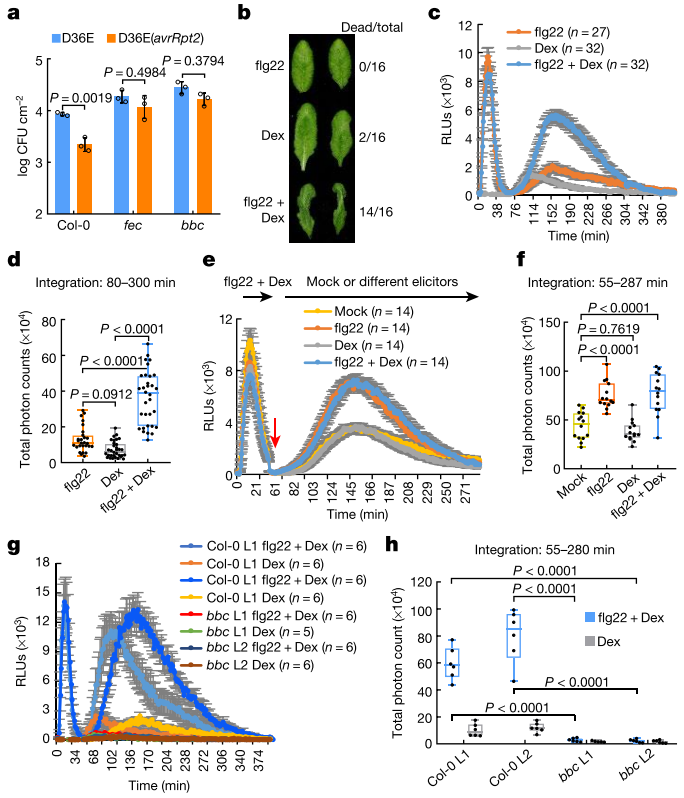

Fig. 1 | PTI-associated PRR/co-receptors are required for ETI responses and resistance. a, D36E(*avrRpt2*) bacteria at an optical density at 600 nm (OD_{600}) of 0.004 were infiltrated and populations were determined 4 days post-infiltration (dpi). Two-way ANOVA with Tukey's test. (mean ± s.d.; $n = 3$ biologically independent samples). **b**, Dexamethasone (Dex)-induced hypersensitive response was accelerated by flg22 co-treatment in Col-0/*Dex:avrRpt2* plants. Pictures were taken approximately 6 h after infiltration of 200 nM flg22, 500 nM dexamethasone or 200 nM flg22 + 500 nM dexamethasone into leaves. **c**–**h**, ROS burst detected by the luminol–horseradish peroxidase approach in Col-0/*Dex:avrRpt2* (**c**–**f**) and *bbc*/*Dex:avrRpt2* plants (**g**, **h**), with treatment with different elicitors. Total photon counts (**d**, **f**, **h**) were calculated from **c**, **e**, **g**, respectively. **e**, **f**, Leaf discs were first treated with flg22 + dexamethasone for 35 min, washed with sterilized water 4 times (red arrow), and then subject to mock treatment (sterilized water) or flg22, dexamethasone or flg22 + dexamethasone treatments. Individual data points (n = numbers of leaf disks as biologically independent samples) are plotted in **d**, **f**, **h**; mean ± s.e.m. in **c**, **e**, **g**. Data were analysed by one-way (**d**, **f**) or two-way (**h**) ANOVA with Tukey's test. RLU, relative luminescence unit. In box plots, the centre line represents the median, box edges delimit lower and upper quartiles and whiskers show the highest and lowest data points. Experiments in this figure were repeated at least three times with similar trends.

For the past few decades, conventional studies of ETI triggered by *Pst* DC3000 carrying avirulent effector genes have been performed in the presence of all 36 endogenous effector genes in *Pst* DC3000. However, this has made it difficult to clearly interpret the relationship between PTI and ETI using wild-type *Pst* DC3000 to deliver avirulent effectors to trigger ETI, owing to the interference with PTI and ETI function by the endogenous *Pst* DC3000 effectors, as reported in many studies[15,16]. We therefore took advantage of the *Pst* DC3000 strain D36E[17], in which all 36 effector genes and coronatine biosynthesis genes are deleted and which is thus expected to activate only PTI, and the D36E(*avrRpt2*) strain, which secretes only AvrRpt2 and activates both PTI and ETI. Although D36E exhibits markedly reduced virulence compared with *Pst* DC3000 (Fig. 1a, Extended Data Fig. 1a), we still observed a robust AvrRpt2-induced ETI in Col-0 plants, with infections with D36E(*avrRpt2*) resulting in significantly less growth than infection with the D36E strain (Fig. 1a). We found that AvrRpt2-triggered ETI was almost undetectable in either *fec* or *bbc* mutants (Fig. 1a).

PRR/co-receptors regulate ROS production in ETI

AvrRpt2 cleaves the *Arabidopsis* protein RPM1-INTERACTING PROTEIN 4 (RIN4), leading to activation of RPS2[10,11]. We found that D36E(*avrRpt2*)-induced RIN4 protein depletion and the *RPS2* transcript level were not affected in the *fec* and *bbc* mutants (Extended Data Fig. 2a,b). We also observed normal ETI-associated phosphorylation of MPK3 and MPK6 (that is, at 4 h or 8 h after inoculation) in *fec* and *bbc* mutants (Extended Data Fig. 2c).

PTI and ETI have been associated with production of ROS, a key immune function that has been proposed to act in defence, killing pathogens and as signalling molecules that further activate immune responses[18]. We examined PTI- and ETI-associated ROS production in transgenic *Dex:avrRpt2* plants, in which *avrRpt2* expression is driven by a dexamethasone-inducible promoter[19]. In this system, PTI and ETI can be initiated separately or in combination using pathogen-associated molecular patterns (PAMPs) (such as flg22, a 22-amino-acid peptide derived from bacterial flagellin) and dexamethasone treatments. We found that flg22 treatment accelerates the AvrRpt2-triggered hypersensitive response, which is especially noticeable at early time points (5–6 h) (Fig. 1b). Furthermore, whereas flg22 alone triggered a fast and transient ROS burst within 35 min (hereafter referred to as PTI^{ROS}) (Fig. 1c), dexamethasone-induced expression of AvrRpt2 alone triggered only a weak and kinetically slower ROS burst. Of note, co-treatment with both flg22 and dexamethasone triggered a strong and sustained second-phase ROS burst (hereafter ETI^{ROS}), peaking at 2–3 h after treatment and lasting for several hours (Fig. 1c, d), a profile that bears a strong similarity to previous observations during bacteria-triggered ETI[20,21]. To determine whether the second peak of ETI^{ROS} requires sustained active PTI signalling, we washed off the solution containing flg22 and dexamethasone after the first ROS peak (that is, after 35 min), subsequently adding sterilized water, flg22, dexamethasone or both flg22 and dexamethasone (Extended Data Fig. 3a). The results show that ETI^{ROS} requires newly added flg22 (Fig. 1e, f), suggesting that continued PTI signalling during the second phase is important for ETI^{ROS}. We further tested the requirement of PTI signalling for ETI^{ROS} by generating *bbc/Dex:avrRpt2* and Col-0/*Dex:avrRpt2* plants (Extended Data Fig. 3b). In the *bbc/Dex:avrRpt2* plants, there was no flg22-induced first-phase ROS and the ETI^{ROS} was almost completely abolished, clearly demonstrating a requirement of PRR/co-receptor signalling for ETI^{ROS} production (Fig. 1g, h).

To examine whether PTI- and ETI-associated ROS bursts are produced at the same or different subcellular compartments, we monitored ROS production with the fluorescent dye H_2DCFDA[22]. We detected a strong fluorescent signal in the apoplastic spaces of Col-0 leaves 5 h after infiltration of D36E(*avrRpt2*) (Fig. 2a). This signal was much weaker in the *bbc* mutant leaves, which were indistinguishable from *rps2* control leaves infiltrated with D36E(*avrRpt2*) or Col-0 leaves infiltrated with D36E (Fig. 2a). Two classes of enzymes, the NADPH oxidases and peroxidases, have been shown to be involved in generating pathogen-associated apoplastic ROS[23,24]. We therefore investigated which class is involved in the generation of ETI^{ROS} by using chemical inhibitors diphenylene iodonium (DPI), which inhibits NADPH oxidases, and salicylhydroxamic acid (SHAM) and sodium azide, which inhibit peroxidase activities[20,25]. As shown in Extended Data Fig. 4a–c, co-treatment of DPI, but not SHAM or sodium azide, with flg22 and dexamethasone greatly diminished ETI^{ROS}. When we added these inhibitors at 40 min after flg22 + dexamethasone treatment (that is, after PTI^{ROS} and before the start of ETI^{ROS}), DPI, but not SHAM or sodium azide, greatly diminished ETI^{ROS} (Extended Data Fig. 4d), indicating that NADPH oxidases mediate ETI^{ROS}. We further tested whether

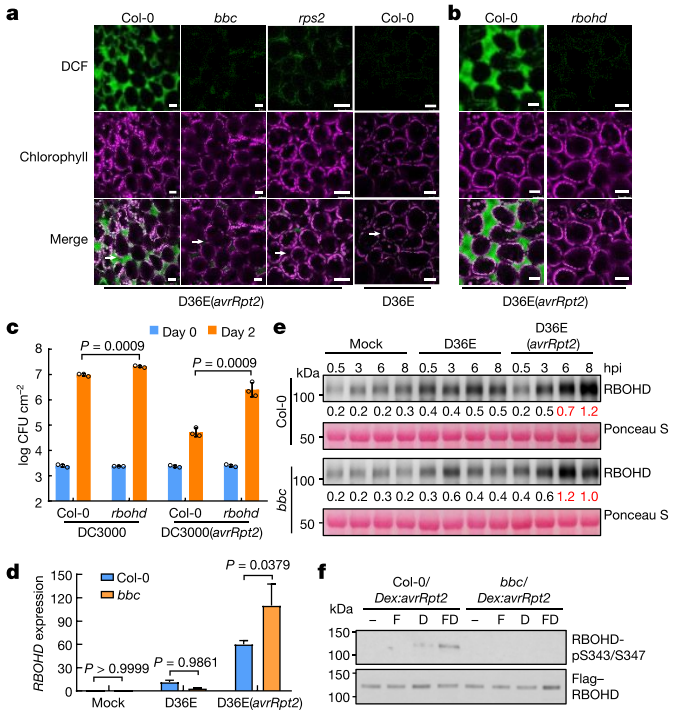

Fig. 2 | AvrRpt2-triggered ROS is mediated by RBOHD and requires PRR/co-receptors. a, **b**, ROS burst detected with the fluorescent dye H_2DCFDA (DCF) in Col-0, *bbc*, *rps2* and *rbohd* leaves 5 h after infiltration of D36E(*avrRpt2*) or in Col-0 leaves 5 h after infiltration of the D36E strain. White arrows indicate the apoplast space in the leaf. Scale bars, 25 µm. **c**, *Pst* DC3000 (*avrRpt2*) bacteria were infiltrated at an OD_{600} of 0.001 and bacterial populations were determined at 2 dpi. Data were analysed by two-tailed Student's *t*-test. Data are mean ± s.d. ($n = 3$ biologically independent samples). **d**, **e**, RBOHD transcript (**d**) and protein (**e**) levels in Col-0 and *bbc* plants 3 h (**d**) or different time points (**e**) after inoculation of indicated bacterial strains. **d**, Data are mean ± s.e.m. $n = 4$ biologically independent samples for *bbc*-Mock/D36E and Col-0-D36E, and $n = 3$ biologically independent samples for Col-0-Mock/D36E(*avrRpt2*) and *bbc*-D36E(*avrRpt2*). Data were analysed by two-way ANOVA with Tukey's test. *P* values for additional comparisons are provided in Supplementary Table 3. **e**, Numbers indicate band intensity relative to that of Ponceau S, quantified by ImageJ. **f**, Phosphorylation of RBOHD protein at S343/S347 sites (RBOHD-pS343/S347). Flag–RBOHD was transformed into protoplasts, which were then treated with elicitors (–, mock treatment; F, 100 nM flg22; D, 5 µM dexamethasone; FD, 100 nM flg22 + 5 µM dexamethasone) and collected 2.5 h later for Flag–RBOHD immunoprecipitation and protein blotting. Experiments in this figure were repeated at least three times with similar trends. Gel source data are shown in Supplementary Fig. 1.

RESPIRATORY BURST OXIDASE HOMOLOGUE D (RBOHD), which has a prominent role in generating pathogen-induced ROS[23,26,27], mediates the ETI^{ROS}. As shown in Fig. 2b, D36E(*avrRpt2*)-induced apoplastic ROS was completely lost in the *rbohd* plant. The *rbohd* plant also showed a compromised ETI resistance against *Pst* DC3000(*avrRpt2*) (Fig. 2c, Extended Data Fig. 5a, b). Together, these results suggest that RBOHD is a key molecular node connecting PTI and ETI.

RBOHD activation in PTI and ETI

We next assayed the transcript and protein levels of RBOHD and found that they are induced both by D36E and, to a much higher level, by D36E(*avrRpt2*) inoculation in Col-0 plants (Fig. 2d, e). However, this strong induction of *RBOHD* transcript and protein by D36E(*avrRpt2*) also occurred in *bbc* mutant plants (Fig. 2d, e), suggesting an involvement of post-translational regulation of RBOHD by PRR signalling during ETI. Previous studies have reported several classes of kinases,

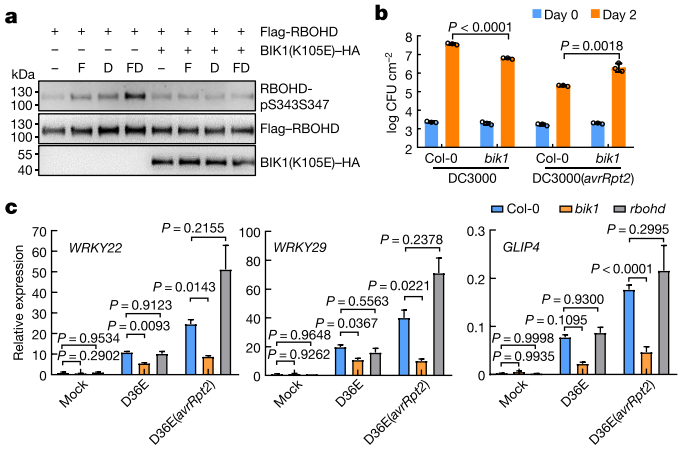

Fig. 3 | BIK1 is required for phosphorylation of RBOHD, immune gene expression and resistance during ETI. a, Phosphorylation of RBOHD at S343/S347 sites during ETI. Protoplasts from Col-0/*Dex:avrRpt2* plants were transformed with DNA constructs expressing Flag–RBOHD and/or BIK1(K105E)–HA as indicated, followed by treatment with 100 nM flg22 (F), 5 µM dexamethasone (D) or 100 nM flg22 + 5 µM dexamethasone (FD) for 2.5 h before immunoprecipitation and protein blotting. **b**, *Pst* DC3000(*avrRpt2*) bacteria were infiltrated into *Arabidopsis* leaves at an OD_{600} of 0.001 and bacterial populations were determined at 2 dpi. Data were analysed by two-tailed Student's *t*-test. Data are mean ± s.d. ($n = 3$ biologically independent samples). **c**, RT–qPCR analysis of *WRKY22*, *WRKY29* and *GLIP4* expression level in Col-0, *bik1* and *rbohd* plants 3 h after mock treatment or infiltration with indicated bacterial strains. Data are mean ± s.e.m. ($n = 4$ biologically independent samples); analysed by two-way ANOVA with Tukey's test. Experiments were repeated at least three times with similar trends. Gel source data are shown in Supplementary Fig. 1.

including CALCIUM DEPENDENT PROTEIN KINASES (CPKs) and *BOTRYTIS*-INDUCED KINASE 1 (BIK1), involved in phosphorylating RBOHD for ROS production[18]. We found that ETI^{ROS} was reduced in the *bik1* mutant, which was readily observed when *bik1* plants were grown in 0.5× Murashige–Skoog agar plates, but did not seem to be affected in the *cpk5 cpk6 cpk11* mutant (Extended Data Fig. 6a, b). BIK1 rapidly and transiently (that is, 15 min after elicitation) phosphorylates RBOHD at multiple sites including S39, S343 and S347 during PTI[26,27]. We therefore examined RBOHD phosphorylation levels during PTI and/or ETI in protoplasts prepared from Col-0/*Dex:avrRpt2* and *bbc/Dex:avrRpt2* plants and transformed them with a DNA construct expressing Flag–RBOHD. A 35S promoter was used to express Flag–RBOHD to ensure similar protein levels during various treatments. We found that dexamethasone alone reproducibly induced a modest phosphorylation of RBOHD S343/S347 in Col-0/*Dex:avrRpt2* leaf protoplasts 2.5 h after treatment (Fig. 2f), whereas combined flg22 and dexamethasone treatment induced a much stronger phosphorylation on S343/S347 (Fig. 2f). By contrast, no phosphorylation was detected in the *bbc* background with any of the treatments, confirming the requirement of PRR/co-receptor signalling for RBOHD phosphorylation during ETI. We further observed that the phosphorylation of RBOHD at S343/347 during ETI is BIK1-dependent, by examining S343/S347 phosphorylation in protoplasts expressing BIK1(K105E)–HA, a kinase-dead and dominant-negative BIK1[27] (Fig. 3a), and that ETI-associated restriction of *Pst* DC3000(*avrRpt2*) growth was significantly compromised in the *bik1* mutant (Fig. 3b, Extended Data Fig. 5c, d). S343/S347 phosphorylation of RBOHD has previously been shown to be important for ETI resistance and restriction of bacterial growth[28]. These results highlight the importance of PRR and NLR signalling in the coordination of the abundance (that is, by NLR signalling) and full activity (that is, by PRR–BIK1 signalling) of RBOHD for generating robust ETI^{ROS}.

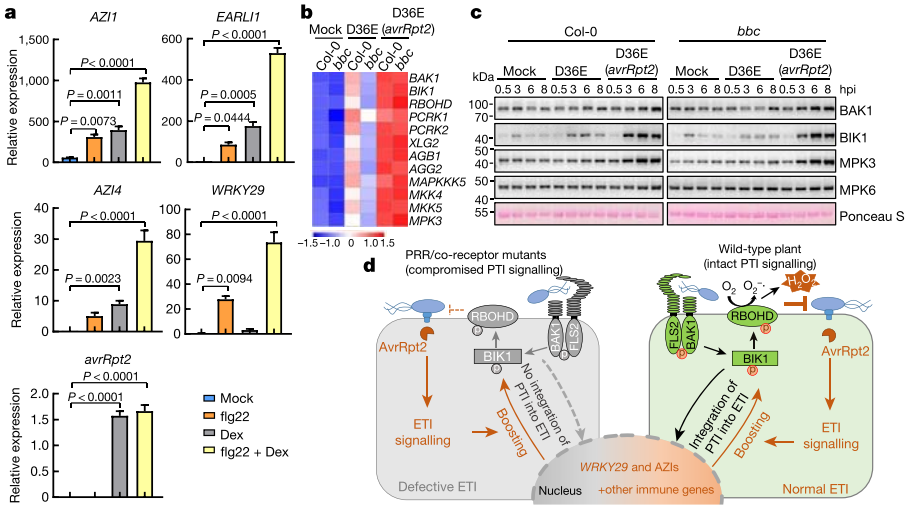

Fig. 4 | ETI upregulates key components of the PTI pathway. a, Expression levels of *avrRpt2*, *WRKY29*, *AZI1*, *EARLI1* and *AZI4* genes in Col-0/*Dex:avrRpt2* transgenic plants after treatment with different elicitors. Leaves were collected 2 h after infiltration for transcript analysis (mean ± s.e.m.; $n = 3$ biologically independent samples). Dex, dexamethasone. Statistical analysis by one-way ANOVA with Tukey's test. *P* values for additional comparisons are provided in Supplementary Table 3. **b**, Heat map showing expression of PTI pathway genes. **c**, Protein levels of BAK1, BIK1, MPK3 and MPK6 in Col-0 and *bbc* plants at different time points after inoculation with indicated bacterial strains. MPK6 protein is not induced by ETI and serves as an internal control. These experiments were repeated at least three times with similar trends. **d**, Model depicting the findings from this study, showing PTI as a key component of ETI. In wild-type plants, RPS2 activation leads to protein accumulation of key PTI components, including BIK1 and RBOHD, and potentiation of PTI-associated genes such as *WRKY29* and AZIs. PRR/co-receptors are required to fully activate ROBHD (by phosphorylation) to generate robust ROS and normal ETI. In the absence of PRR/co-receptors (left), although NLR activation still induces PTI components, many of these components, such as BIK1 and RBOHD, are inactive, leading to lack of ROS production and defective ETI. Mutated (that is, FLS2 and BAK1) or inactive (that is, RBOHD and BIK1) proteins are coloured grey and active proteins are in green. Gel source data are shown in Supplementary Fig. 1.

PTI- and ETI-associated transcriptomes

The requirement of PTI signalling for activation of RBOHD and a strong upregulation of RBOHD during ETI (Fig. 2d, e) suggested that ETI may have evolved to co-opt RBOHD and other components of the PTI pathway as an integral part of its signalling mechanism. We therefore examined the expression patterns of other components of the PTI pathway and the rest of the *Arabidopsis* transcriptome using RNA-sequencing analysis (RNA-seq) (Extended Data Fig. 7a, b). Three hours after infiltration, D36E(*avrRpt2*) already caused global differential expression relative to D36E infiltration in Col-0 plants (Extended Data Fig. 7c), suggesting that 3 h is sufficient for delivery of AvrRpt2 into the plant cell and triggering ETI-associated gene expression. Many genes are differentially regulated between Col-0 and *bbc* plants at this early time point in response to PTI-inducing D36E (Extended Data Fig. 7d). Of note, the majority of these genes show similar expression pattern in Col-0 and *bbc* plants after D36E(*avrRpt2*) inoculation (Extended Data Fig. 7d), suggesting that ETI can largely restore PTI-associated global gene expression in *bbc* plants. Similar trends were observed for genes associated with salicylic acid, jasmonate and ethylene pathways (Extended Data Fig. 7e–g). A subset of 272 genes were differentially expressed in *bbc* plants after D36E(*avrRpt2*) inoculation (Supplementary Table 1). In particular, a cluster of WRKY genes including *WRKY22*, *WRKY29* and *FRK1*—canonical marker genes of flg22-induced PTI pathway[29]—are downregulated in the *bbc* plant (Extended Data Fig. 8a, b). This suggests that WRKY–FRK1 represents a distinct branch of the immune system, the activation of which during ETI requires PRR/co-receptors. BIK1, but not RBOHD, was necessary for the full expression of several examined genes, such as *WRKY22* and *WRKY29*, after D36E(*avrRpt2*) inoculation (Fig. 3c). This suggests that BIK1 is one of the integration points for ETI^{ROS} burst and a subset of immune gene expression during ETI. Gene-expression analysis in the Col-0/*Dex:avrRpt2* and *bbc*/*Dex:avrRpt2* plants confirmed ETI-mediated boosting of immune gene expression (for example, *WRKY29*, *AZI1*, *EARLI1* and *AZI4*[30]) (Fig. 4a) and suggested a basal role of PRR/co-receptors per se in ETI-associated gene expression in the absence of PRR signalling activation by flg22 (Extended Data Fig. 8c).

Increase of key PTI components in ETI

Further analysis of PTI- and ETI-associated transcriptomes revealed a characteristic expression pattern for many PTI signalling genes. We found that PTI-inducing D36E moderately induced many key PTI components, namely *BAK1*, *BIK1*, *XLG2*, *AGB1*, *AGG2*[31], *MAPKKK5*, *MKK4*, *MKK5* and *MPK3*, that are associated with RLK and RLP-initiated pathways. However, ETI-inducing D36E(*avrRpt2*) induced much higher levels of these genes (Fig. 4b, Extended Data Fig. 9a). Similar to *RBOHD*, the strong induction of these PTI components by ETI was independent of PRR/co-receptors, as it also occurred in the *bbc* mutant. Upregulation of PRR-encoding genes such as *FLS2*, *EFR* and *LYK5*[2] was not observed during AvrRpt2-induced ETI in bacteria-infected Col-0 plants (Extended Data Fig. 9a), but was observed in transgenic plants expressing AvrRpt2 or AvrRps4 (see the Article by Ngou et al.[32] in this issue). This difference may reflect different ETI-signal input strengths. Nevertheless, the robust upregulation of common co-receptors and other early signalling components, instead of individual PRRs, may represent an evolutionally 'smart' way that enables plants to strengthen immunity irrespective of the specific type of pathogen. Notably, *BIK1* and some other BIK1/PBL family members—but not *PBL1*—are strongly induced after D36E(*avrRpt2*) inoculation (Extended Data Fig. 9b), suggesting differential contribution of different members of the BIK1/PBL family to ETI. Quantitative PCR with reverse transcription (RT–qPCR) and western blot analysis confirmed the upregulation of several key PTI components during ETI in Col-0 and *bbc* plants (Fig. 4c, Extended Data Fig. 10a). Our results, together with those in ref. [32], suggest that ETI signalling rapidly induces high-level expression of key components of the PTI pathway, including BAK1, BIK1 and RBOHD. Further analysis showed that this 're-enforcement' of the PTI pathway during AvrRpt2-induced ETI also

occurs in the salicylic acid biosynthesis mutant *sid2* (Extended Data Fig. 10b) and, furthermore, our RNA-seq results showed that salicylic acid- (Extended Data Fig. 7e) and *N*-hydroxy-pipecolic acid- (Extended Data Fig. 10c) responsive genes were expressed at similar levels in Col-0 and *bbc* plants during ETI.

Discussion

Our study reveals a requirement of PRR/co-receptor signalling for effective ETI and supports a mechanistic model in which ETI co-opts part of the PTI machinery as an indispensable component (Fig. 4d). In particular, we found that PRRs and NLRs, the two primary classes of plant immune receptors, function synergistically to ensure a fully active status as well as a robust level of key immune components, including the BIK1–RBOHD module, which mediates ETI^{ROS} generation, full immunity-associated gene expression and disease resistance during ETI. A synergistic interaction between cell surface and intracellular immune receptors in animals and humans has also been reported[33], suggesting a possible conceptual parallel in immune receptor functions across different kingdoms of life. Our study sheds light on a long-standing question in the field of plant immunity regarding the similarity between PTI- and ETI-associated cellular features. The results could have broad practical implications, as they suggest the possibility of using carefully controlled augmentation of PTI components as a strategy to broadly increase the effectiveness of ETI against many diseases in crop plants.

Online content

Any methods, additional references, Nature Research reporting summaries, source data, extended data, supplementary information, acknowledgements, peer review information; details of author contributions and competing interests; and statements of data and code availability are available at https://doi.org/10.1038/s41586-021-03316-6.

1. Yu, X., Feng, B., He, P. & Shan, L. From chaos to harmony: responses and signaling upon microbial pattern recognition. *Annu. Rev. Phytopathol.* **55**, 109–137 (2017).
2. Couto, D. & Zipfel, C. Regulation of pattern recognition receptor signalling in plants. *Nat. Rev. Immunol.* **16**, 537–552 (2016).
3. Spoel, S. H. & Dong, X. How do plants achieve immunity? Defence without specialized immune cells. *Nat. Rev. Immunol.* **12**, 89–100 (2012).
4. Cui, H., Tsuda, K. & Parker, J. E. Effector-triggered immunity: from pathogen perception to robust defense. *Annu. Rev. Plant Biol.* **66**, 487–511 (2015).
5. Jones, J. D. & Dangl, J. L. The plant immune system. *Nature* **444**, 323–329 (2006).
6. Chisholm, S. T., Coaker, G., Day, B. & Staskawicz, B. J. Host–microbe interactions: shaping the evolution of the plant immune response. *Cell* **124**, 803–814 (2006).
7. Jones, J. D., Vance, R. E. & Dangl, J. L. Intracellular innate immune surveillance devices in plants and animals. *Science* **354**, aaf6395 (2016).
8. Tsuda, K. & Katagiri, F. Comparing signaling mechanisms engaged in pattern-triggered and effector-triggered immunity. *Curr. Opin. Plant Biol.* **13**, 459–465 (2010).
9. Peng, Y., van Wersch, R. & Zhang, Y. Convergent and divergent signaling in pamp-triggered immunity and effector-triggered immunity. *Mol. Plant Microbe Interact.* **31**, 403–409 (2018).
10. Axtell, M. J. & Staskawicz, B. J. Initiation of RPS2-specified disease resistance in *Arabidopsis* is coupled to the AvrRpt2-directed elimination of RIN4. *Cell* **112**, 369–377 (2003).
11. Mackey, D., Belkhadir, Y., Alonso, J. M., Ecker, J. R. & Dangl, J. L. *Arabidopsis* RIN4 is a target of the type III virulence effector AvrRpt2 and modulates RPS2-mediated resistance. *Cell* **112**, 379–389 (2003).
12. Xin, X. F. et al. Bacteria establish an aqueous living space in plants crucial for virulence. *Nature* **539**, 524–529 (2016).
13. Shao, F. et al. Cleavage of *Arabidopsis* PBS1 by a bacterial type III effector. *Science* **301**, 1230–1233 (2003).
14. Gassmann, W., Hinsch, M. E. & Staskawicz, B. J. The *Arabidopsis* RPS4 bacterial-resistance gene is a member of the TIR–NBS–LRR family of disease-resistance genes. *Plant J.* **20**, 265–277 (1999).
15. Xin, X. F., Kvitko, B. & He, S. Y. *Pseudomonas syringae*: what it takes to be a pathogen. *Nat. Rev. Microbiol.* **16**, 316–328 (2018).
16. Toruño, T. Y., Stergiopoulos, I. & Coaker, G. Plant-pathogen effectors: cellular probes interfering with plant defenses in spatial and temporal manners. *Annu. Rev. Phytopathol.* **54**, 419–441 (2016).
17. Wei, H. L. et al. *Pseudomonas syringae pv. tomato* DC3000 type III secretion effector polymutants reveal an interplay between HopAD1 and AvrPtoB. *Cell Host Microbe* **17**, 752–762 (2015).
18. Qi, J., Wang, J., Gong, Z. & Zhou, J. M. Apoplastic ROS signaling in plant immunity. *Curr. Opin. Plant Biol.* **38**, 92–100 (2017).
19. McNellis, T. W. et al. Glucocorticoid-inducible expression of a bacterial avirulence gene in transgenic *Arabidopsis* induces hypersensitive cell death. *Plant J.* **14**, 247–257 (1998).
20. Levine, A., Tenhaken, R., Dixon, R. & Lamb, C. H_2O_2 from the oxidative burst orchestrates the plant hypersensitive disease resistance response. *Cell* **79**, 583–593 (1994).
21. Chandra, S., Martin, G. B. & Low, P. S. The Pto kinase mediates a signaling pathway leading to the oxidative burst in tomato. *Proc. Natl Acad. Sci. USA* **93**, 13393–13397 (1996).
22. Tian, S. et al. Plant aquaporin AtPIP1;4 links apoplastic H_2O_2 induction to disease immunity pathways. *Plant Physiol.* **171**, 1635–1650 (2016).
23. Torres, M. A., Dangl, J. L. & Jones, J. D. *Arabidopsis gp91^{phox}* homologues *AtrbohD* and *AtrbohF* are required for accumulation of reactive oxygen intermediates in the plant defense response. *Proc. Natl Acad. Sci. USA* **99**, 517–522 (2002).
24. Daudi, A. et al. The apoplastic oxidative burst peroxidase in *Arabidopsis* is a major component of pattern-triggered immunity. *Plant Cell* **24**, 275–287 (2012).
25. Li, Y. et al. Glucose triggers stomatal closure mediated by basal signaling through HXK1 and PYR/RCAR receptors in *Arabidopsis*. *J. Exp. Bot.* **69**, 1471–1484 (2018).
26. Kadota, Y. et al. Direct regulation of the NADPH oxidase RBOHD by the PRR-associated kinase BIK1 during plant immunity. *Mol. Cell* **54**, 43–55 (2014).
27. Li, L. et al. The FLS2-associated kinase BIK1 directly phosphorylates the NADPH oxidase RbohD to control plant immunity. *Cell Host Microbe* **15**, 329–338 (2014).
28. Kadota, Y. et al. Quantitative phosphoproteomic analysis reveals common regulatory mechanisms between effector- and PAMP-triggered immunity in plants. *New Phytol.* **221**, 2160–2175 (2019).
29. Asai, T. et al. MAP kinase signalling cascade in *Arabidopsis* innate immunity. *Nature* **415**, 977–983 (2002).
30. Cecchini, N. M., Steffes, K., Schläppi, M. R., Gifford, A. N. & Greenberg, J. T. *Arabidopsis* AZI1 family proteins mediate signal mobilization for systemic defence priming. *Nat. Commun.* **6**, 7658 (2015).
31. Liang, X. et al. *Arabidopsis* heterotrimeric G proteins regulate immunity by directly coupling to the FLS2 receptor. *eLife* **5**, e13568 (2016).
32. Ngou, B. P. M., Ahn, H.-K., Ding, P. & Jones, J. D. G. Mutual potentiation of plant immunity by cell-surface and intracellular receptors. *Nature* https://doi.org/10.1038/s41586-021-03315-7 (2021).
33. Cao, X. Self-regulation and cross-regulation of pattern-recognition receptor signalling in health and disease. *Nat. Rev. Immunol.* **16**, 35–50 (2016).

Methods

No statistical methods were used to predetermine sample size. The experiments were not randomized. The investigators were not blinded to allocation during experiments and outcome assessment.

Plant materials and growth conditions

Arabidopsis thaliana plants used in this study are in Col-0 ecotype background. The *fls2 efr cerk1*[34], *bak1 bkk1 cerk1*[12], *rps2*[35], *rbohd*[23], *bik1*[36], *cpk5 cpk6 cpk11*[37] mutants were previously reported. Plants were grown in potting soil in environmentally controlled growth chambers, with relative humidity set at 60% and temperature at 22 °C with a 12-h light:12-h dark photoperiod unless stated otherwise. Four- to five-week-old plants were used for all experiments in this study. To generate the *bbc/Dex:avrRpt2* and Col-0/*Dex:avrRpt2* transgenic plants, the *avrRpt2* gene was cloned into pBUD-Dex (pBD) vector in the *Xho*I/*Spe*I restriction enzyme sites, and the expression cassette was introduced into Col-0 or *bbc* plants by *Agrobacterium*-mediated transformation. The *bik1* and *rbohd* plants for disease assays were grown on Redi-Earth soil (Sun Gro Horticulture) to minimize growth defect, under relative humidity set at 60%, temperature at 23 °C, light intensity at 100 μE·m2·s and photoperiod at a 12-h light:12-h dark cycle.

Bacterial disease and hypersensitive response assays

The *Pst* DC3000 strains carrying *avrRpt2*, *avrRps4* and *avrPphB* have previously been described[38–40]. The D36E(*avrRpt2*) strain was generated by transforming the *avrRpt2* expression plasmid into D36E strain by electroporation. For bacterial inoculation, *Pst* strains were cultured in a modified Luria–Bertani medium[12] overnight at 30 °C to an OD_{600} of 0.8–1.0. Bacteria were collected by centrifugation and washed once with sterilized water, and adjusted to an OD_{600} of 0.2. For disease assay, bacterial suspension was further diluted to an OD_{600} of 0.001–0.002. Bacteria were infiltrated into leaves with a needleless syringe, and inoculated plants were kept under ambient humidity for about 1 h to allow evaporation of excess water from the leaf and then covered with a transparent plastic dome to keep high humidity for disease to develop. For quantification of bacteria, four leaf discs from two different leaves (after surface sterilization) were taken using a cork borer (7.5 mm in diameter) as one biological repeat, and 3–4 repeats were taken for each treatment (repeat numbers are different across treatments in cases of not sufficient healthy plants). Leaf discs were ground and diluted in sterilized water, and the extraction solutions were then plated on LM agar plates supplemented with rifampicin (at 50 mg l^{-1}). Colonies were counted with a stereoscope 24 h after incubation at 30 °C. For the hypersensitive response assay (HR assay), *Pst* DC3000(*avrRpt2*) suspension was prepared as described above and bacterial suspension at an OD_{600} of 0.2 was syringe-infiltrated into leaves. Plants were then kept under ambient humidity for about 7 h before tissue collapse was recorded. For HR assay in Col-0/*Dex:avrRpt2* plants, four-week-old plant leaves were infiltrated with 200 nM flg22, 500 nM dexamethasone or 200 nM flg22 + 500nM dexamethasone, respectively. Fully-expanded leaves at a similar developmental stage were chosen (about 3 leaves per plant) for treatments. Severely wounded leaves (during infiltration) were discarded in final counting. Infiltrated plants were kept under ambient humidity and pictures were taken 5–6 h after infiltration.

RIN4 cleavage assays

Arabidopsis plant leaves were infiltrated with *Pst* D36E or *Pst* D36E(*avrRpt2*) (at OD_{600} = 0.1), and samples were collected at 0, 2, 4 or 8 h after infiltration by snap-freezing in liquid nitrogen. Three leaves were collected as one biological repeat. Total proteins were extracted in protein extraction buffer (50 mM Tris-HCl pH 7.5, 150 mM NaCl, 5 mM EDTA pH 7.5, 1 mM DTT, 1% Triton X-100, 1 mM phenylmethylsulfonyl fluoride) supplemented with 1× plant protease inhibitor cocktail (Complete EDTA-free, Roche). Cell lysates were centrifuged at 12,000*g* for 15 min at 4 °C, and the pellet was discarded. Protein concentration of the supernatant ('total protein extract') was determined by Bradford protein assay kit (Bio-Rad). An equal amount of total protein was loaded on 12% SDS acrylamide gels (Bio-Rad) for SDS–PAGE. RIN4 protein was detected by anti-RIN4 antibody[41] at a dilution of 1:1,000. Goat anti-rabbit IgG–horseradish peroxidase (HRP) (Abmart; 1:5,000) was used as secondary antibody. The protein image was taken using the Tanon-5200 imaging system (Tanon). Total proteins were stained with Coomassie blue to show equal loading.

MAPK kinase activity assay

Four-week-old plant leaves were infiltrated with *Pst* D36E or *Pst* D36E(*avrRpt2*) (at OD_{600} = 0.02), and leaves were collected at different time points by snap-freezing in liquid nitrogen. Proteins were extracted in protein extraction buffer (50 mM Tris-HCl pH 7.5, 150 mM NaCl, 5 mM EDTA pH 7.5, 1 mM DTT, 1% Triton X-100, 1 mM phenylmethylsulfonyl fluoride) supplemented with 1× plant protease inhibitor cocktail (Complete EDTA-free, Roche) and 1× phosphatase inhibitor cocktail (PhosSTOP, Roche). Total protein concentration was determined with Bradford protein assay kit (Bio-Rad). An equal amount of protein was loaded onto a 12% SDS–PAGE gel for western blot. Phosphorylated MPK3 and MPK6 proteins were detected by anti-phospho-p44/42 antibody (Cell Signaling Technology; 1:1,000). Goat anti-rabbit IgG HRP (Abmart; 1:5,000) was used as secondary antibody. The protein image was taken using the Tanon-5200 imaging system (Tanon).

Protein extraction and immunoblotting for PTI signalling components

Four-week-old plant leaves were infiltrated with sterilized water (mock) or different *Pst* strains at OD_{600} = 0.02, and samples were collected at 0.5, 3, 6 and 8 h after infiltration. Three to four leaves from different plants were collected as one sample. Protein was extracted using Plasma Membrane Protein Isolation Kit (Invent) according to the manufacturer's protocol. Concentration of the cytosolic protein was determined with Bradford protein assay kit (Bio-Rad). An equal amount of protein was loaded onto SDS–PAGE gel for western blot. BAK1 and RBOHD are detected in the immunoblot of total membrane fraction and other proteins are detected in the immunoblot of total protein extracts. Different PTI components were detected by following antibodies with indicated dilution: anti-RBOHD (Agrisera), 1:1,000; anti-BAK1 (Agrisera), 1:5,000; anti-BIK1 (Agrisera), 1:3,000; anti-MPK3 (Sigma-Aldrich), 1:2,500; anti-MPK6 (Sigma-Aldrich), 1:5000. Goat Anti-Rabbit IgG HRP (Abmart; 1:5,000) was used as secondary antibody. The protein image was taken using the Tanon-5200 imaging system (Tanon).

Protoplast transformation and detection of RBOHD phosphorylation

Protoplasts were prepared from Col-0/*Dex:avrRpt2* and *bbc/Dex:avrRpt2* plants (4–5 weeks old; grown under 10-h light:14-h dark photoperiod) and transfected with Flag-RBOHD plasmid. After overnight incubation to allow protein accumulation, protoplasts were treated with 100 nM flg22, 5 μM dexamethasone or 100 nM flg22 + 5 μM dexamethasone and incubated for 2.5 h. Total protein was extracted with protein extraction buffer (50 mM HEPES pH 7.5, 150 mM KCl, 1 mM EDTA, 0.5% Triton-X100, 1 mM DTT, protease inhibitor cocktail), and then incubated with 50 μl anti-Flag M2 agarose beads (Sigma-Aldrich) for 2 h at 4 °C. The bound protein was eluted with 50 μl of 0.5 mg ml^{-1} 3× Flag peptide for 30 min. Total RBOHD was detected with Flag antibody (Sigma-Aldrich; 1:5,000). RBOHD phosphorylation was detected by immunoblotting with RBOHD-pS343/347 antibody published previously[27]. To determine whether BIK1 is important for phosphorylating RBOHD during ETI, Col-0/*Dex:avrRpt2* transgenic plants were grown under the 10-h light:14-h dark photoperiod for 4 to 5 weeks, and protoplasts were prepared (from 40–50 fully expanded leaves) and transformed with Flag–RBOHD plasmid alone or co-transformed with

Flag–RBOHD and BIK1(K105E)–HA plasmids[27]. After elicitor treatment (see above), total proteins were extracted using the protein extraction buffer (50 mM HEPES (pH 7.5), 150 mM NaCl, 5 mM EDTA, 0.5% Triton-X100, 0.1% IGEPAL CA-630, 10% glycerol, 1 mM DTT, protease inhibitor cocktail and PhosSTOP cocktail) by incubating protoplasts with extraction buffer on ice for 1 h. Supernatant was collected after centrifugation at 12,000 rpm at 4 °C for 20 min and incubated with 50 µl anti-Flag M2 agarose beads (Sigma-Aldrich) for 2.5 h at 4 °C. The bound proteins were eluted with 120 µl of 0.3 mg ml^{-1} 3× Flag peptide (Sigma-Aldrich) after incubation at 4 °C for 1 h. RBOHD phosphorylation was detected by immunoblotting using the RBOHD-pS343/347 antibody (1:1,000), and BIK1(K105E)–HA was detected using the anti-HA antibody (Abmart). Goat anti-rabbit IgG–HRP (Abmart; 1:5,000) or goat anti-mouse IgG HRP (Abmart; 1:5,000) were used as secondary antibody. The protein image was taken using the Tanon-5200 imaging system (Tanon).

ROS detection

ROS measurement with luminol-based approach was performed as previously described with minor modification[26]. In brief, leaf discs of four-week-old *Arabidopsis* plants were collected using a cork borer (5.5 mm in diameter) and floated on 200 µl sterilized water in a 96-well plate, and then incubated overnight at room temperature under continuous light. On the next day, water was replaced with a solution containing 30 mg l^{-1} (w/v) luminol (Sigma-Aldrich) and 20 mg l^{-1} (w/v) peroxidase from horseradish (Sigma-Aldrich) with 100 nM flg22 only, 5 µM dexamethasone only or 100 nM flg22 + 5 µM dexamethasone. The luminescence was detected for 5–6 h with a signal integration time of 1 or 2 min using Varioskan Flash plate reader (Thermo Fisher Scientific) and analysed with SkanIt Software (Thermo Scientific; 6.0). To determine the effects of chemical inhibitors, 10 µM diphenyleneiodonium (DPI; Sigma-Aldrich), 15 µM salicylhydroxamic acid (Sigma-Aldrich) or 1 µM sodium azide was added to the elicitation solution at indicated time points and luminescence was recorded as described above. To examine whether co-treatment of flg22 and dexamethasone is important for production of ETI^{ROS}, leaf discs from Col-0/*Dex:avrRpt2* transgenic plants were first treated with flg22+ dexamethasone for 35 min, during which the production of ROS was detected by a microplate reader. Then the leaf discs were washed with sterilized water 4 times, 5 min each time with gentle agitation of leaf disc-containing plates. Then sterilized water (mock), 100 nM flg22, 5 µM dexamethasone or 100 nM flg 22 + 5 µM dexamethasone was added to the leaf discs and ROS burst was recorded. For detection of ROS production by 2′,7′-dichlorofluorescein diacetate (H_2DCFDA) under confocal microscopy, plants were infiltrated with *Pst* D36E (OD_{600} = 0.02) or D36E(*avrRpt2*) (OD_{600} = 0.02), air-dried and put back into the plant growth room. ROS was detected at 4–5 h post infiltration. Ten micromolar H_2DCFDA solution was infiltrated into the leaf and fluorescence signal was detected 10 min later. Images were captured using a Leica SP8 microscope with a 488 nm excitation and 501–550 nm emission, and chlorophyll auto-fluorescence was detected at 640–735 nm.

RNA extraction and RT–qPCR analysis of gene expression

To analyse gene-expression levels, four-week-old *Arabidopsis* plant leaves were infiltrated with sterilized water (mock) or different *Pst* strains at OD_{600} = 0.04, and then collected at indicated time points. Three leaves from different plants were collected as one biological replicate and four replicates were collected for each treatment. For analysis of genes expression in Col-0/*Dex:avrRpt2* plants, leaves from four-week-old plants (grown under the 10-h:14-h light:dark photoperiod) were infiltrated with 20 nM flg22, 50 nM dexamethasone or 20 nM flg22 + 50 nM dexamethasone, respectively. We used low concentrations of elicitors, which are presumed to be closer to the physiological level, so that induction of gene expression by either pathway alone is not saturated and the individual contribution and a possible synergistic effect of PTI and ETI can be observed. At 2 h after infiltration, two leaves from two different plants were collected as one biological replicate for gene transcript analysis (replicate numbers are different across treatments in cases of not sufficient healthy plants). Samples were frozen and ground in liquid nitrogen. Total mRNA was extracted using Trizol reagent (Invitrogen) according to the manufacturer's protocol. One microgram of RNA was used for reverse transcription using the ReverTra Ace qPCR RT Master Mix with gDNA remover (TOYOBO). Real-time qPCR analysis was carried out with the SYBRGreen Realtime PCR Master Mix (TOYOBO) on a CFX real-time machine (Bio-Rad). Two technical repeats were performed for each sample. The plant *U-BOX* gene was used as reference gene for normalization. Primer sequences for quantitative PCR are listed in Supplementary Table 2.

cDNA library generation and RNA-seq

For RNA-seq experiments, bacterial inoculation and sample collection were performed as described above. Two leaves from different plants were collected as one replicate, and four biological replicates were collected for each treatment and time point. Total mRNA was extracted using Trizol reagent (Invitrogen). Total RNA was then treated with DNase I (Invitrogen) to remove DNA and purified RNA was recovered with RNeasy MinElute Cleanup kit (QIAGEN) according to the manufacturer's instructions. Library construction and RNA sequencing were performed by Novogene company. In brief, RNA purity and integrity was examined using the NanoPhotometer spectrophotometer (IMPLEN) and the RNA Nano 6000 Assay Kit of the Bioanalyzer 2100 system (Agilent Technologies). RNA concentration was measured with Qubit RNA Assay Kit in Qubit 2.0 Flurometer (Life Technologies). One microgram RNA per sample was used as input material for library preparation and sequencing. Sequencing libraries were generated using NEBNext Ultra RNA Library Prep Kit for Illumina (NEB), following the manufacturer's recommendations and sequenced on Illumina Hiseq platform and 150-bp paired-end reads were generated.

Data analysis of RNA-seq

Clean raw data were obtained by removing reads containing adaptor sequences or ploy-N and low-quality reads and were then mapped to the *Arabidopsis* genome (TAIR10). Gene-expression levels were calculated using the transcripts per kb of exon model per million mapped reads (TPM) method. Differential expression analysis was performed using the DESeq R package (1.18.0). The resulting *P* values were adjusted using the Benjamini and Hochberg's approach for controlling the false discovery rate. Genes with a *q*-value <0.05 and $\log_2$(fold change) >1 found by DESeq were assigned as differentially expressed.

Statistical analysis

All statistical analyses were performed by one-way or two-way ANOVA with GraphPad software or by two-sided Student's *t*-test with Office Excel software. Each experiment was repeated at least three times and data were represented as the mean ± s.e.m. or s.d. as indicated.

Reporting summary

Further information on research design is available in the Nature Research Reporting Summary linked to this paper.

Data availability

The RNA-seq data have been deposited into the NCBI Gene Expression Omnibus under accession GSE142747. All data are available in the main text or the supplementary materials. Source data are provided with this paper.

34. Gimenez-Ibanez, S., Ntoukakis, V. & Rathjen, J. P. The LysM receptor kinase CERK1 mediates bacterial perception in *Arabidopsis*. *Plant Signal. Behav.* **4**, 539–541 (2009).

35. Mindrinos, M., Katagiri, F., Yu, G. L. & Ausubel, F. M. The *A. thaliana* disease resistance gene *RPS2* encodes a protein containing a nucleotide-binding site and leucine-rich repeats. *Cell* **78**, 1089–1099 (1994).
36. Veronese, P. et al. The membrane-anchored *BOTRYTIS-INDUCED KINASE1* plays distinct roles in *Arabidopsis* resistance to necrotrophic and biotrophic pathogens. *Plant Cell* **18**, 257–273 (2006).
37. Gao, X. et al. Bifurcation of *Arabidopsis* NLR immune signaling via Ca^{2+}-dependent protein kinases. *PLoS Pathog.* **9**, e1003127 (2013).
38. Mudgett, M. B. & Staskawicz, B. J. Characterization of the *Pseudomonas syringae pv. tomato* AvrRpt2 protein: demonstration of secretion and processing during bacterial pathogenesis. *Mol. Microbiol.* **32**, 927–941 (1999).
39. Hinsch, M. & Staskawicz, B. Identification of a new *Arabidopsis* disease resistance locus, *RPs4*, and cloning of the corresponding avirulence gene, avrRps4, from *Pseudomonas syringae pv. pisi*. *Mol. Plant Microbe Interact.* **9**, 55–61 (1996).
40. Aarts, N. et al. Different requirements for EDS1 and NDR1 by disease resistance genes define at least two R gene-mediated signaling pathways in *Arabidopsis*. *Proc. Natl Acad. Sci. USA* **95**, 10306–10311 (1998).
41. Lee, D., Bourdais, G., Yu, G., Robatzek, S. & Coaker, G. Phosphorylation of the plant immune regulator RPM1-INTERACTING PROTEIN4 enhances plant plasma membrane H^+-ATPase activity and inhibits flagellin-triggered immune responses in *Arabidopsis*. *Plant Cell* **27**, 2042–2056 (2015).
42. Pajerowska-Mukhtar, K. M. et al. The HSF-like transcription factor TBF1 is a major molecular switch for plant growth-to-defense transition. *Curr. Biol.* **22**, 103–112 (2012).
43. Hickman, R. et al. Architecture and dynamics of the jasmonic acid gene regulatory network. *Plant Cell* **29**, 2086–2105 (2017).
44. Nemhauser, J. L., Hong, F. & Chory, J. Different plant hormones regulate similar processes through largely nonoverlapping transcriptional responses. *Cell* **126**, 467–475 (2006).
45. Hartmann, M. et al. Flavin monooxygenase-generated *N*-hydroxypipecolic acid is a critical element of plant systemic immunity. *Cell* **173**, 456–469 (2018).

Acknowledgements We thank Xin laboratory members for helpful discussions; the Greenhouse and Confocal Microscopy Imaging facilities at the CAS Center for Excellence in Molecular Plant Sciences for plant growth and technical support; G. Coaker from University of California, Davis for providing the RIN4 antibody; B. P. M. Ngou and P. Ding from J. Jones' laboratory at the Sainsbury Laboratory for insightful discussions during manuscript preparation. This research was supported by the Chinese Academy of Sciences, Center for Excellence in Molecular Plant Sciences/Institute of Plant Physiology and Ecology, National Key Laboratory of Plant Molecular Genetics and Chinese Academy of Sciences Strategic Priority Research Program (Type-B; project number: XDB27040211). G.B. was supported by the Youth Program of National Natural Science Foundation of China (NSFC) (project number: 31900222). The initial observation of PRR dependency for ETI resistance was made by X.-F.X. while at Michigan State University, supported by the US National Institute of General Medical Sciences (GM109928, to S.Y.H.).

Author contributions M.Y. and X.-F.X. conceptualized and designed experiments at the CAS Center for Excellence in Molecular Plant Sciences/Institute of Plant Physiology and Ecology. M.Y. performed most experiments, including ROS detection, disease/HR assays, RNA-seq, and transcript and protein analysis. Z.J. and M.L. performed RIN4 cleavage, MAPK phosphorylation and gene-expression experiments. G.B., Y.W., M.Y. and B.C. performed protoplast experiments for detecting RBOHD phosphorylation. K.N. performed the disease assay and gene-expression analysis in *bik1* and *rbohd* mutants. S.Y.H. and J.-M.Z. supervised K.N. and G.B., respectively. M.Y. and X.-F.X. wrote the paper and S.Y.H. and J.-M.Z. edited the paper.

Competing interests The authors declare no competing interests.

Additional information

Supplementary information The online version contains supplementary material available at https://doi.org/10.1038/s41586-021-03316-6.

Correspondence and requests for materials should be addressed to X.-F.X.

Peer review information *Nature* thanks Thorsten Nürnberger and the other, anonymous, reviewer(s) for their contribution to the peer review of this work.

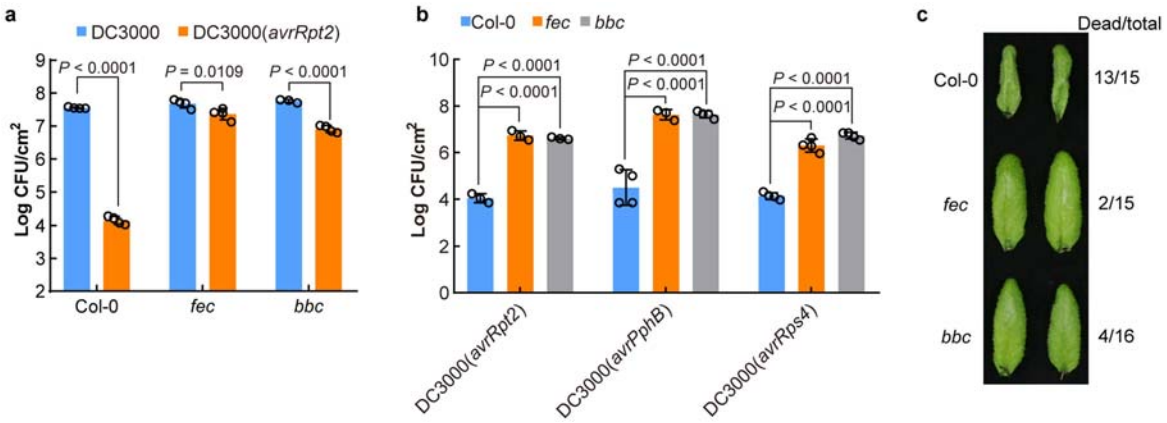

Extended Data Fig. 1 | PRR/co-receptors are required for ETI elicited by different *P. syringae* avirulent effectors. a, *Pst* DC3000 (*avrRpt2*) bacteria were infiltrated into *Arabidopsis* leaves at OD_{600} of 0.002 and populations were determined at 3 dpi (mean ± s.d.; $n = 4$ biologically independent samples, except $n = 3$ biologically independent samples for *bbc*-DC3000). Data were analysed using two-way ANOVA with Tukey's test. **b**, AvrPphB- and AvrRps4-mediated ETI are also compromised in *fec* and *bbc* mutants. Plants were infiltrated with different strains at OD_{600} of 0.002. Bacterial populations were determined 3 dpi. Data were analysed using two-way ANOVA with Tukey's test. (mean ± s.d.; $n = 3$ (Col-0 *fec*/*bbc*-DC3000(*avrRpt2*) and *fec*-DC3000(*avrPphB*)) or 4 (Col-0 *fec*/*bbc*-DC3000(*avrRps4*) and Col-0/*bbc*-DC3000(*avrPphB*)) biologically independent samples). **c**, Hypersensitive response was compromised in PRR/co-receptor mutants. *Pst* DC3000 (*avrRpt2*) bacteria were infiltrated at OD_{600} of 0.2 and images were taken about 7 h post infiltration (hpi). Experiments were repeated three times with similar trends.

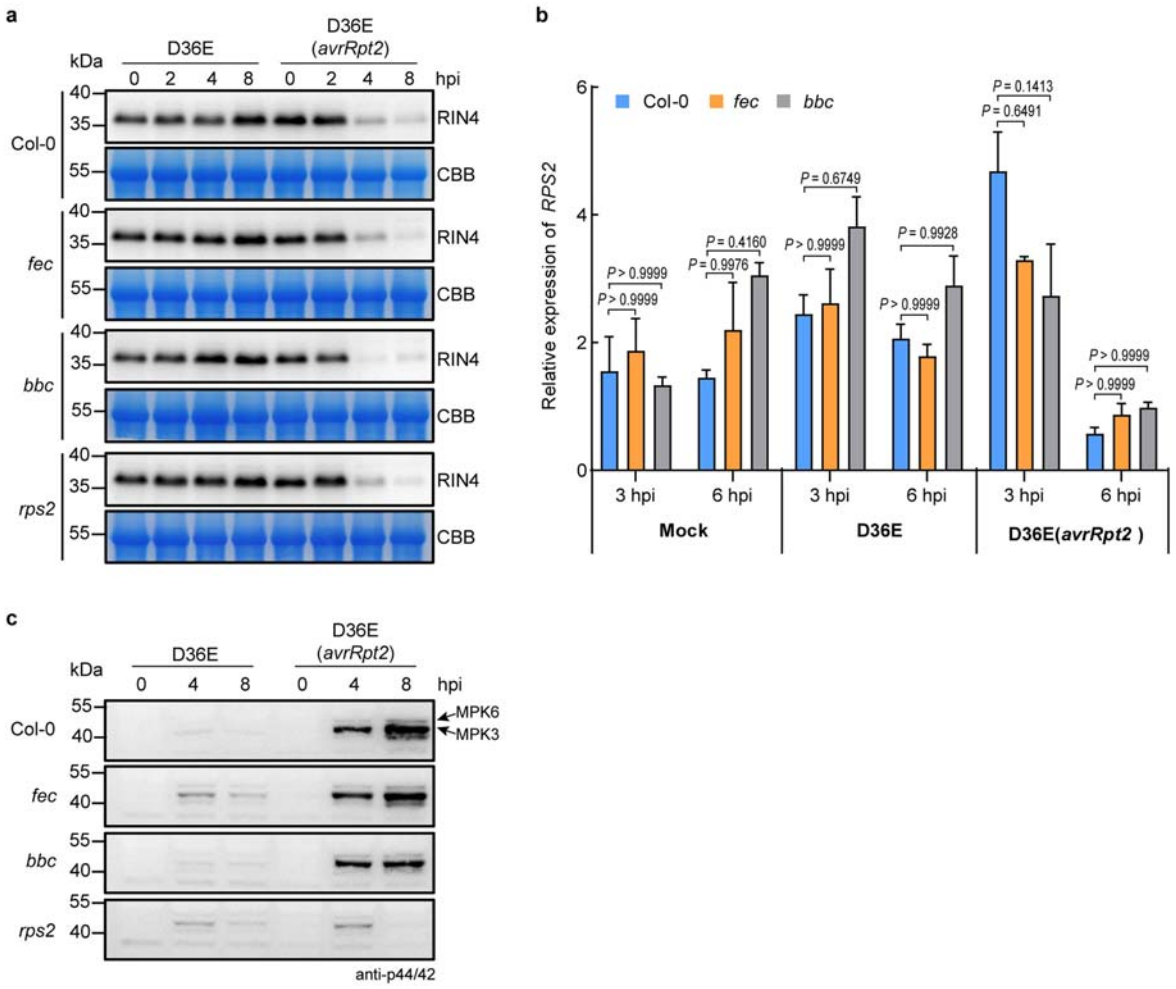

Extended Data Fig. 2 | RIN4 cleavage, transcript level of *RPS2* and activation of MAPK cascades are not altered in the *fec* and *bbc* plants. a, RIN4 cleavage in Col-0 and the PRR/co-receptor mutants after D36E or D36E(*avrRpt2*) inoculation. CBB, Coomassie blue staining. An equal amount of total protein was loaded in each lane. **b**, *RPS2* transcript levels in the *fec* and *bbc* mutant plants were similar to those in Col-0 plants after inoculation of indicated bacterial strains. Statistical analysis was performed using two-way ANOVA with Tukey's test. (mean ± s.e.m.; $n = 3$ biologically independent samples). **c**, Phosphorylation of MPK3 and MPK6 (MPK3/6) in Col-0 and the PRR/co-receptor mutants after D36E or D36E(*avrRpt2*) inoculation. An equal amount of total protein was loaded in each lane. Experiments were repeated at least three times with similar trends. For gel source data, see Supplementary Fig. 1.

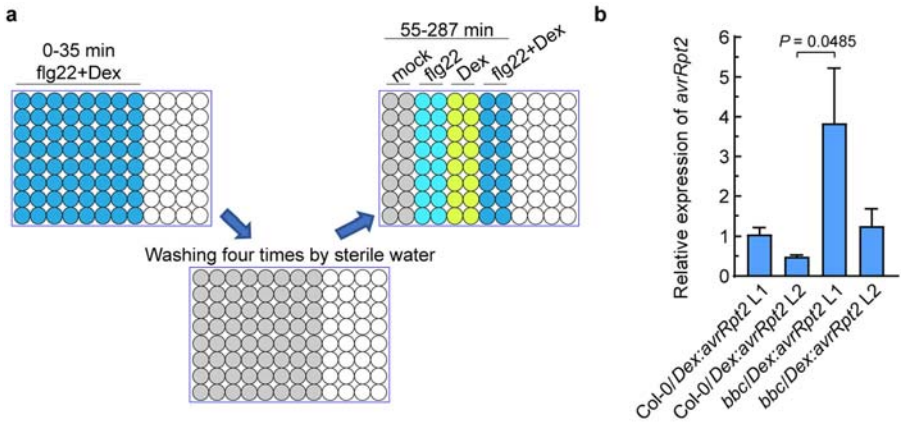

Extended Data Fig. 3 | Characterization of different lines of *bbc*/*Dex:avrRpt2* plants. a, Schematic of the experimental design. Leaf discs were first treated with flg22 + dexamethasone (Dex) for 35 min, and the production of ROS was detected by a microplate reader. Leaf discs were then washed with sterilized water 4 times, for 5 min each time. Sterilized water (mock treatment), 100 nM flg22, 5 μM dexamethasone or 100 nM flg22 + 5 μM dexamethasone was then added for detection of second-phase ROS. **b**, Expression levels of the *avrRpt2* transgene in different transgenic lines 2 h after infiltration with 5 μM dexamethasone. Statistical analysis was performed using one-way ANOVA with Tukey's test (mean ± s.e.m.; $n = 3$ (Col-0/*Dex:avrRpt2* L2, *bbc*/*Dex:avrRpt2* L1, *bbc*/*Dex:avrRpt2* L2) or 4 (Col-0/*Dex:avrRpt2* L1) biologically independent samples). Experiments were repeated three times with similar trends.

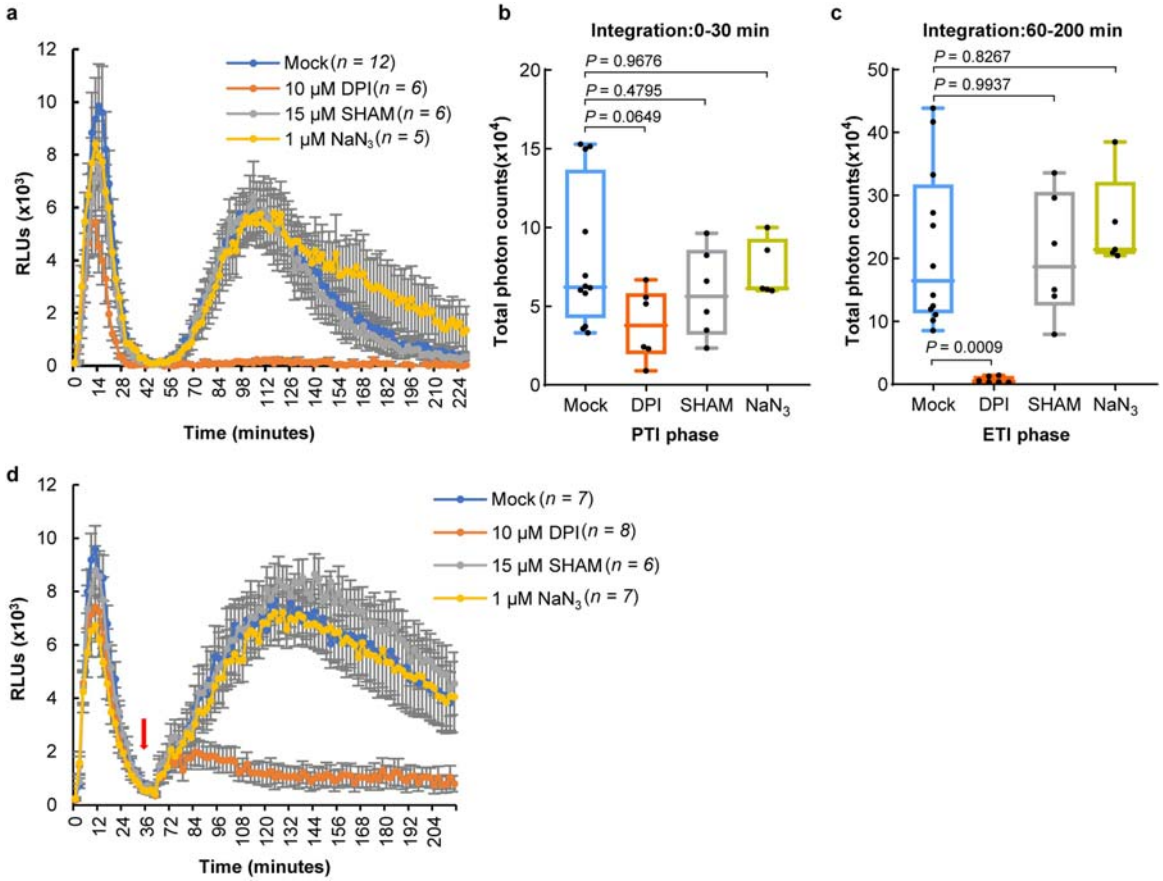

Extended Data Fig. 4 | AvrRpt2-triggered ETI^{ROS} depends on NADPH oxidase. a–**c**, ROS production in Col-0/*Dex:avrRpt2* L1 plants was inhibited by NADPH oxidase inhibitor DPI. Leaf discs were treated with 100 nM flg22 and 5 μM dexamethasone (Dex). DPI, SHAM and NaN_3 were added at the beginning of measurement (mean ± s.e.m.; *n* (numbers of leaf discs) are indicated in the panel). **b**, **c**, Total photon counts are calculated from **a** at the PTI phase (0–30 min) or ETI phase (60–200 min). Statistical analysis was performed by one-way ANOVA with Tukey's test. **d**, ETI-associated ROS burst is inhibited by DPI, an NADPH oxidase inhibitor. ROS was detected in Col-0/*Dex:avrRpt2* plants after treatment with 100 nM flg22 and 5 μM dexamethasone. Chemical inhibitors (DPI, SHAM or NaN_3) were added after the first ROS burst (about 40 min after addition of flg22 and dexamethasone). Data are mean ± s.e.m. *n* (numbers of leaf discs) is indicated in the panel. In box plots the centre line represents the median, box edges delimit lower and upper quartiles and whiskers show the highest and lowest data points. Experiments in this figure were repeated three times with similar trends.

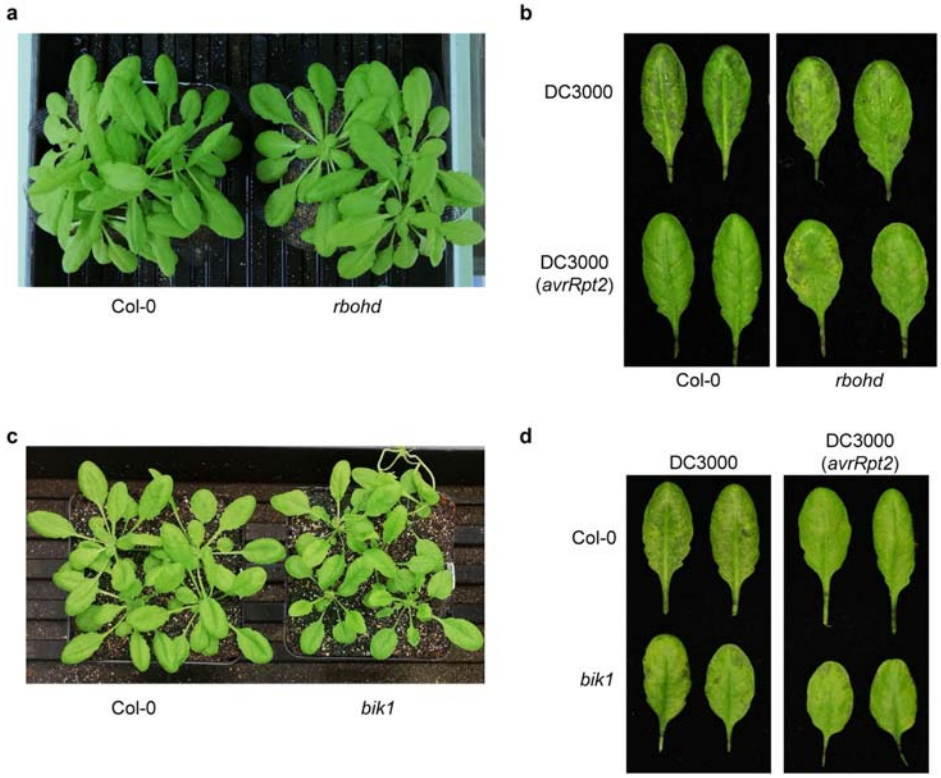

Extended Data Fig. 5 | The *rbohd* and *bik1* mutant plants are compromised in ETI resistance against *Pst* DC3000 (*avrRpt2*). **a**, Appearance of the 5 week-old *rbohd* mutant plants before bacteria inoculation. **b**, Disease symptom of Col-0 and *rbohd* mutant plant 2 days after *Pst* DC3000 and *Pst* DC3000 (*avrRpt2*) infiltration. **c**, Appearance of the 4.5 week-old *bik1* mutant plants growth in Redi-Earth soil before bacteria inoculation. **d**, Disease symptoms of Col-0 and *bik1* mutant plant 2 days after *Pst* DC3000 and *Pst* DC3000 (*avrRpt2*) infiltration. Experiments in this figure were repeated three times with similar trends.

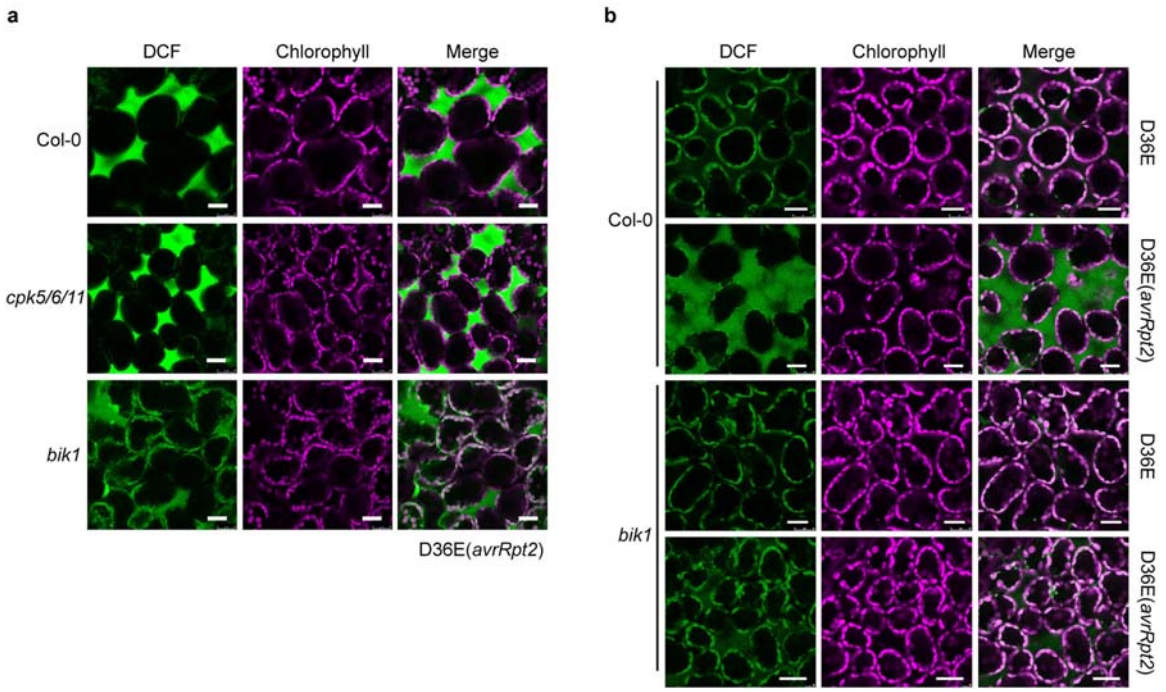

Extended Data Fig. 6 | The AvrRpt2 ETI-associated ROS burst is partially mediated by BIK1. a, ROS was detected in the *bik1* and *cpk5 cpk6 cpk11* mutant plants by H_2DCFDA dye 4.5 h after D36E(*avrRpt2*) inoculation. Scale bars, 25 µm. **b**, ROS was detected in the *bik1* mutant plants by H_2DCFDA dye 5 h after D36E or D36E(*avrRpt2*) inoculation. Plants were grown on 0.5× Murashige–Skoog plates for 3 weeks. Scale bars, 25 µm. Experiments in this figure were repeated three times with similar trends.

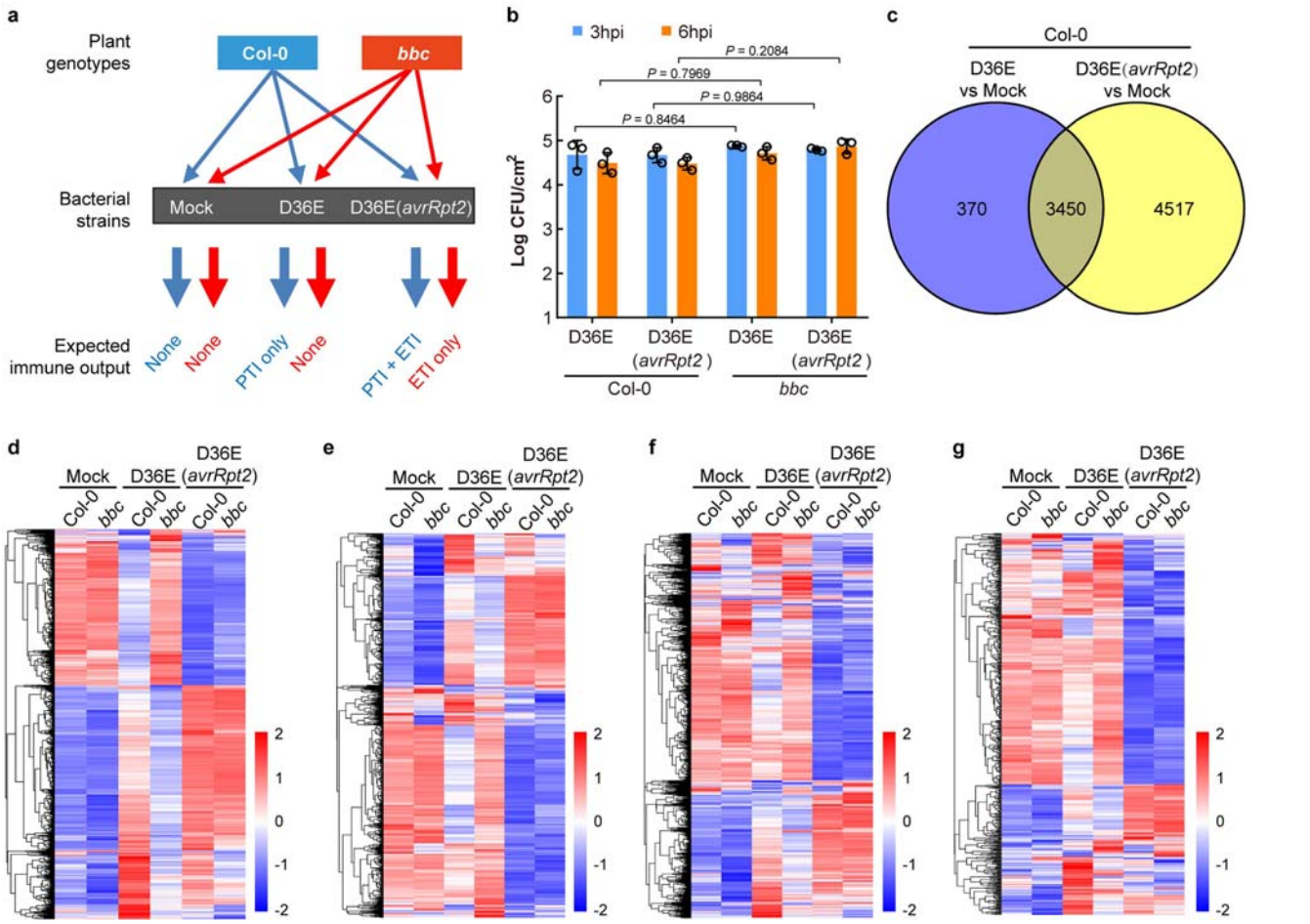

Extended Data Fig. 7 | Transcriptomic analysis of RNA-seq experiments. **a**, A diagram showing the RNA-seq design in this study. **b**, Bacterial population in *Arabidopsis* leaves at 3 h or 6 h post infiltration. Data are mean ± s.d. ($n = 3$ biologically independent samples). Statistical analysis was performed using two-way ANOVA with Tukey's test. **c**, A Venn diagram showing numbers of differentially expressed genes (DEGs) 3 h after D36E or D36E(*avrRpt2*) infection in Col-0 plants. **d**, Heat map of the expression pattern of D36E/PTI-responsive genes. **e**–**g**, Heat maps of salicylic acid-responsive (**e**; genes extracted from ref. [42]), jasmonate-responsive (**f**; genes extracted from ref. [43]) and ethylene-responsive (**g**; genes extracted from ref. [44]) genes.

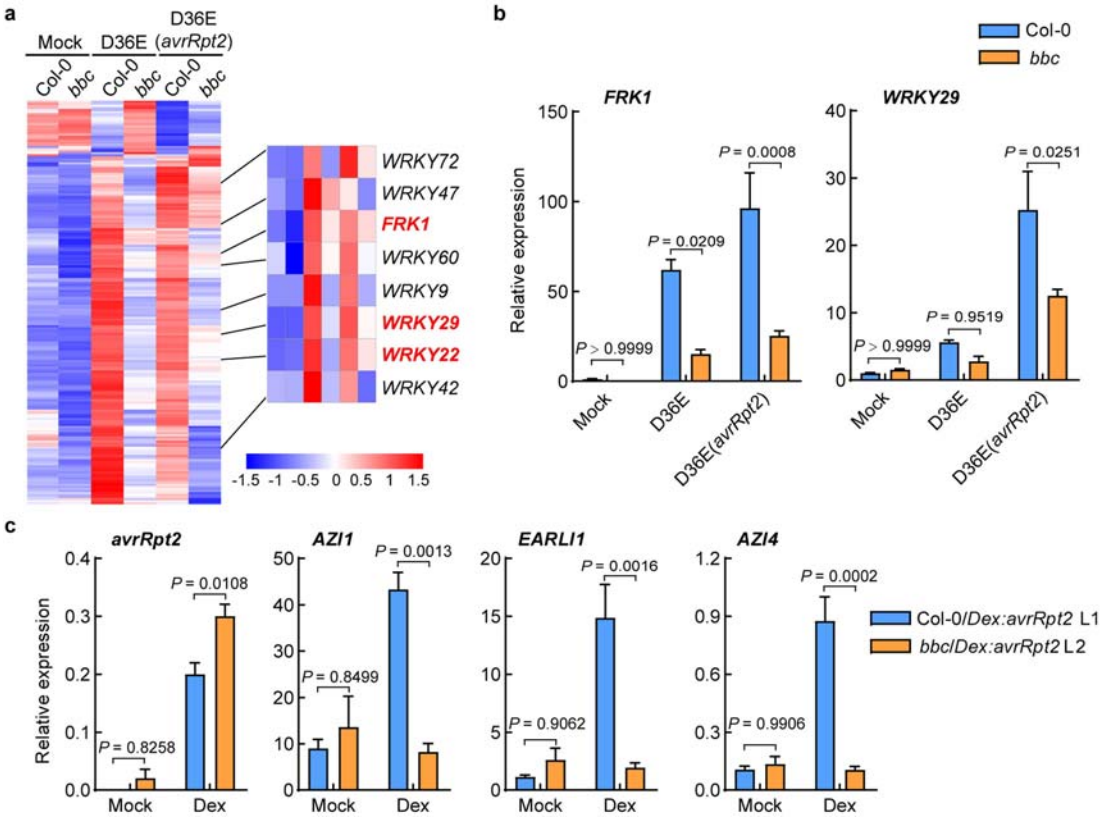

Extended Data Fig. 8 | PRR/co-receptors are important for immune-related gene expression. a, **b**, *WRKY–FRK1* is a unique immune branch and cannot be restored by ETI in the *bbc* mutant. **a**, Heat map of the 272 DEGs in the *bbc* plant compared to Col-0 plant after D36E(*avrRpt2*) infection, with the canonical PTI pathway genes highlighted in red. **b**, RT–qPCR of *FRK1* and *WRKY29* expression level in Col-0 and *bbc* plants 3 h after infiltration with different strains or mock treatment (mean ± s.e.m.; $n = 3$ biologically independent samples; statistical analysis by two-way ANOVA with Tukey's test). **c**, Expression level of *avrRpt2*, *AZI1*, *EARLI1* and *AZI4* in the Col-0/*Dex:avrRpt2* L1 and *bbc*/*Dex:avrRpt2* L2 plants after sterilized water (mock) or dexamethasone (Dex, 50 nM for Col-0/*Dex:avrRpt2* and 100 nM for *bbc*/*Dex:avrRpt2*) treatment. Leaves were collected 2 h post-infiltration for transcript analysis (mean ± s.e.m.; $n = 3$ biologically independent samples; statistical analysis by two-way ANOVA with Tukey's test). Experiments in **b** and **c** were repeated at least three times with similar trends.

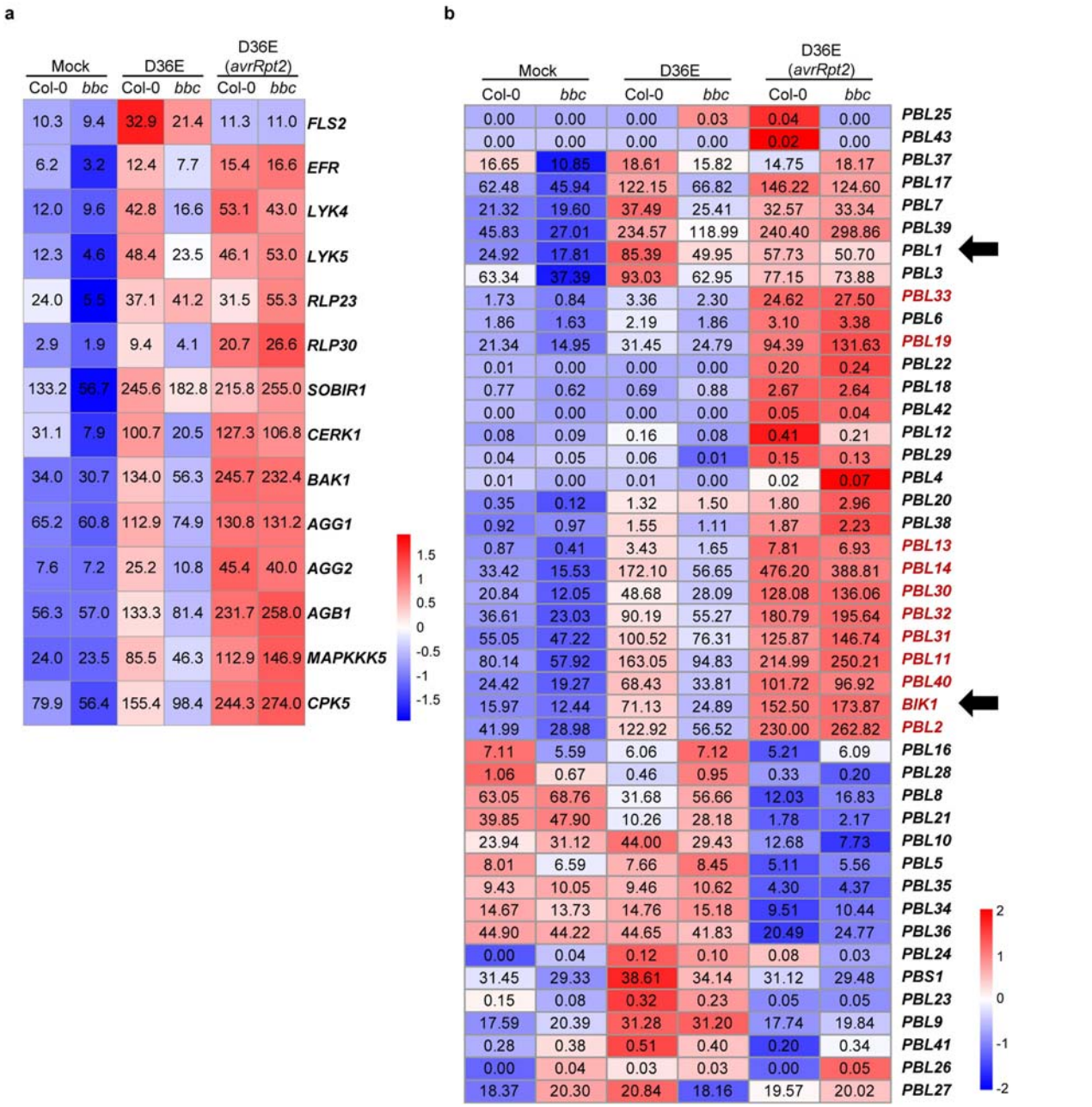

Extended Data Fig. 9 | Heat map of *RLK–LYK5–RLP*-pathway and BIK1/PBL family gene expression. a, *RLK–LYK5–RLP*-pathway gene expression by RNA-seq. **b**, BIK1/PBL family gene expression by RNA-seq. Numerical values indicate expression level calculated as TPM. Genes labelled in red show significant upregulation after D36E(*avrRpt2*) inoculation, compared to mock and D36E inoculation, in Col-0 and *bbc* plants. Arrows in **b** indicate *BIK1* and *PBL1* genes.

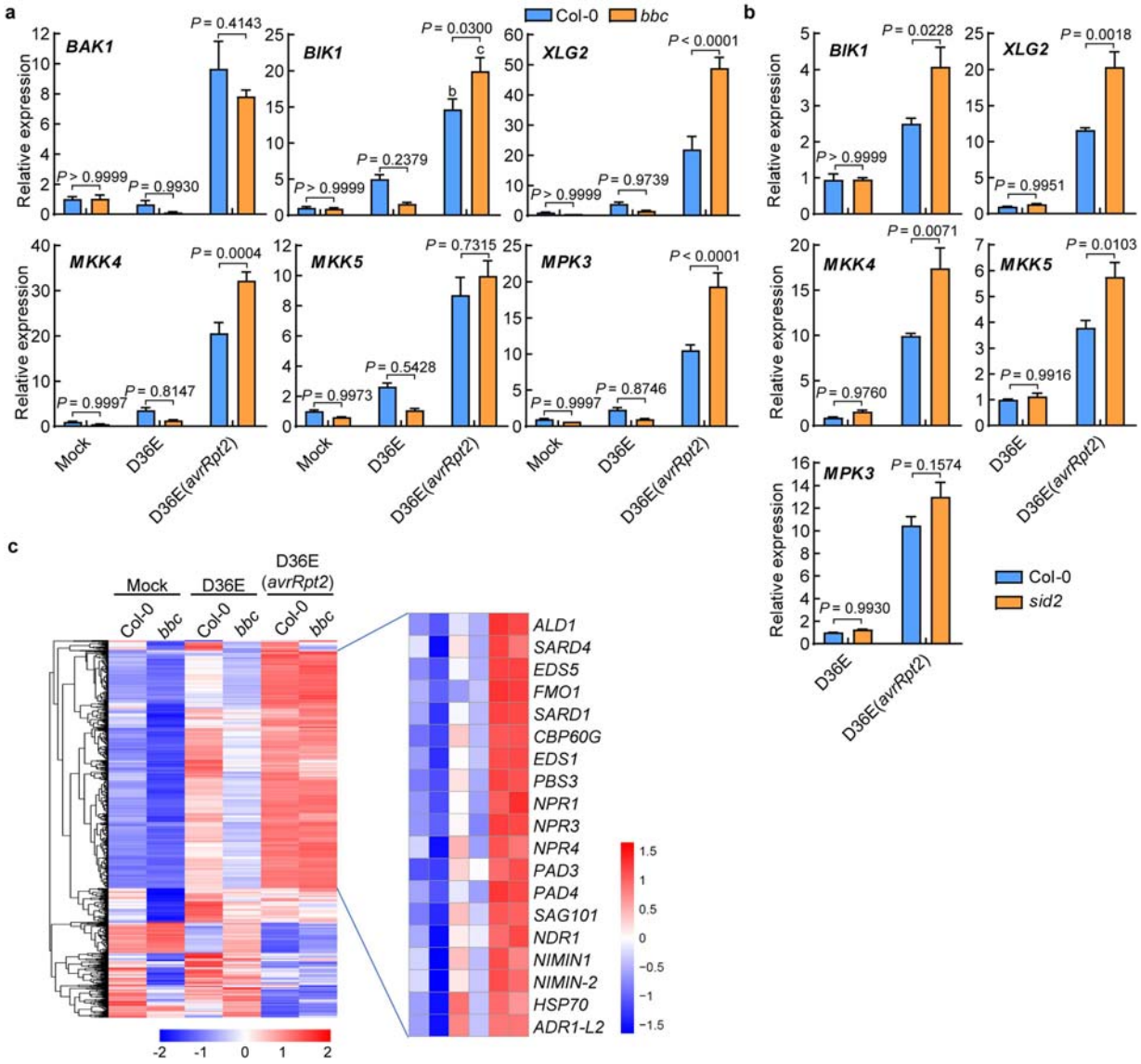

Extended Data Fig. 10 | Upregulation of key PTI component genes by AvrRpt2-triggered ETI seems to be independent of PTI and salicylic acid–*N*-hydroxy-pipecolic acid. a, RT–qPCR results of representative PTI-pathway genes. Col-0 and *bbc* plants were infiltrated with different strains indicated, and leaves were collected 3 h post infiltration for transcript analysis (mean ± s.e.m.; $n = 3$ biological replicates for all plants or genes; except *bbc-BAK1*, $n = 4$ biologically independent samples). Statistical analysis by two-way ANOVA with Tukey's test. *P* values for additional comparisons are provided in Supplementary Table 3. **b**, RT–qPCR analysis of *BIK1*, *XLG2*, *MKK4*, *MKK5* and *MPK3* expression levels in Col-0 and *sid2* plants 3 h after infiltration with D36E or D36E(*avrRpt2*). Statistical analysis by two-way ANOVA with Tukey's test (mean ± s.e.m.; $n = 3$ (for Col-0) or 4 (for *sid2*) biologically independent samples). These experiments were repeated at least three times with similar trends. **c**, Heat maps of *N*-hydroxy-pipecolic acid-responsive genes (extracted from ref. [45], defined by genes that are responsive to pipecolic acid and depend on FMO1 for expression) in the Col-0 and *bbc* plants in our RNA-seq experiment.

nature research

Corresponding author(s): Xiu-Fang Xin

Last updated by author(s): Jan 24, 2021

Reporting Summary

Nature Research wishes to improve the reproducibility of the work that we publish. This form provides structure for consistency and transparency in reporting. For further information on Nature Research policies, see our Editorial Policies and the Editorial Policy Checklist.

Statistics

For all statistical analyses, confirm that the following items are present in the figure legend, table legend, main text, or Methods section.

n/a	Confirmed	
☐	☒	The exact sample size (*n*) for each experimental group/condition, given as a discrete number and unit of measurement
☐	☒	A statement on whether measurements were taken from distinct samples or whether the same sample was measured repeatedly
☐	☒	The statistical test(s) used AND whether they are one- or two-sided *Only common tests should be described solely by name; describe more complex techniques in the Methods section.*
☒	☐	A description of all covariates tested
☐	☒	A description of any assumptions or corrections, such as tests of normality and adjustment for multiple comparisons
☐	☒	A full description of the statistical parameters including central tendency (e.g. means) or other basic estimates (e.g. regression coefficient) AND variation (e.g. standard deviation) or associated estimates of uncertainty (e.g. confidence intervals)
☐	☒	For null hypothesis testing, the test statistic (e.g. *F*, *t*, *r*) with confidence intervals, effect sizes, degrees of freedom and *P* value noted *Give P values as exact values whenever suitable.*
☒	☐	For Bayesian analysis, information on the choice of priors and Markov chain Monte Carlo settings
☒	☐	For hierarchical and complex designs, identification of the appropriate level for tests and full reporting of outcomes
☒	☐	Estimates of effect sizes (e.g. Cohen's *d*, Pearson's *r*), indicating how they were calculated

Our web collection on statistics for biologists contains articles on many of the points above.

Software and code

Policy information about availability of computer code

Data collection	SkanIt™ Software (Thermo Scientific; 6.0); Leica SP8 microscope(Leica); Tanon-5200(Tanon)
Data analysis	EXCEL16 software(Microsoft); SkanIt™ Software (Thermo Scientific; 6.0); ImageJ(1.47v); LAS AF software(2.6.0 build 7266); Graphpad Prism software(8.0.1); DESeq R package (1.18.0)

For manuscripts utilizing custom algorithms or software that are central to the research but not yet described in published literature, software must be made available to editors and reviewers. We strongly encourage code deposition in a community repository (e.g. GitHub). See the Nature Research guidelines for submitting code & software for further information.

Data

Policy information about availability of data

All manuscripts must include a data availability statement. This statement should provide the following information, where applicable:

- Accession codes, unique identifiers, or web links for publicly available datasets
- A list of figures that have associated raw data
- A description of any restrictions on data availability

The RNAseq data has been deposited into GEO (Gene Expression Omnibus) repository on NCBI (GSE142747). All data is available in the main text or the supplementary materials. Source data for western blots and graphs in main figures and Extended Data Figures are provided in Supplementary Figure 1 (i.e., uncropped gels for western blots) and Source Data files (i.e., original data points for graphs).

Field-specific reporting

Please select the one below that is the best fit for your research. If you are not sure, read the appropriate sections before making your selection.

☒ Life sciences ☐ Behavioural & social sciences ☐ Ecological, evolutionary & environmental sciences

For a reference copy of the document with all sections, see nature.com/documents/nr-reporting-summary-flat.pdf

Life sciences study design

All studies must disclose on these points even when the disclosure is negative.

Sample size	The sample size and the results of statistical analyses are described in the relevant figure legends or methods section. Sample size was determined based on experimental trials and with consideration of previous publications (Tian et al.,2019.,Nature.,572:131-135; Xiao et al.,2019.,Nature., 572:270-274; Perraki et al.,2018.,Nature.,561:248-252; Dressano et al.,2020., Nat. Plants.,6:1008-1019) on similar experiments to allow for confident statistical analyses.
Data exclusions	No data were excluded.
Replication	Each experiment was repeated at least three times. Results were reproducible in all repeats with the same trend.
Randomization	Plants of different genotypes were grown side by side to minimize unexpected environmental variations during growth and experimentation. Leaf samples of similar ages were collected randomly for all experiments.
Blinding	The investigators were not blinded to group allocation during experiment performing and data analysis. The research materials are plants so the blinding design is not applicable in the field (partially because different plant genotypes may grow differently and show different morphology, making blinding impossible). Experiments were conducted based on routine practice in the field and all experiments were repeated at least three times with similar trends. Experiments were repeated by different authors, whenever possible.

Reporting for specific materials, systems and methods

We require information from authors about some types of materials, experimental systems and methods used in many studies. Here, indicate whether each material, system or method listed is relevant to your study. If you are not sure if a list item applies to your research, read the appropriate section before selecting a response.

Materials & experimental systems

n/a	Involved in the study
☐	☒ Antibodies
☒	☐ Eukaryotic cell lines
☒	☐ Palaeontology and archaeology
☒	☐ Animals and other organisms
☒	☐ Human research participants
☒	☐ Clinical data
☒	☐ Dual use research of concern

Methods

n/a	Involved in the study
☒	☐ ChIP-seq
☒	☐ Flow cytometry
☒	☐ MRI-based neuroimaging

Antibodies

Antibodies used	Commercial antibodies used: Anti-Phospho-p44/42 antibody (Phospho-p44/43 MAPK(Erk1/2)(Thr202/Tyr204) Antibody; Catalog number: #9101; Cell Signaling Technology; 1:1000), Anti-RBOHD (Catalog number: AS152962; Agrisera; 1:1000), Anti-BAK1 (Catalog number: AS121858; Agrisera; 1:5000), Anti-BIK1 (Catalog number: AS164030; Agrisera); 1:3000), Anti-MPK3 (Catalog number: M8318; Sigma-Aldrich; 1:2500), Anti-MPK6 (Catalog number: A7104; Sigma-Aldrich; 1:5000), Anti-Flag(Catalog number: F3165; Sigma-Aldrich; 1:5000), Anti-HA(Catalog number: M20003L; Abmart; 1:5000) Goat Anti-Rabbit IgG HRP(Catalog number: M21002L; Abmart; 1:5000) Goat Anti-Mouse IgG HRP(Catalog number: M21001L; Abmart; 1:5000) Non-commercial antibodies used: Anti-RIN4 antibody at a dilution of 1:1000 (Kindly provided by Dr. Gitta Coaker from University of California, Davis, USA) Anti-pSer343pSer347 antibody at a dilution of 1:1000(Kindly provided by Dr. Jian-Min Zhou from Institute of Genetics and Developmental Biology, Chinese Academy of Sciences, Beijing, China.)

Validation

Anti-Phospho-p44/42 antibody manufacturer's website: https://www.cellsignal.com/products/primary-antibodies/phospho-p44-42-mapk-erk1-2-thr202-tyr204-antibody/9101
Anti-RBOHD antibody manufacturer's website: https://www.agrisera.com/en/artiklar/rbohd-respiratory-burst-oxidase-homolog-protein-d-.html
Anti-BAK1 antibody manufacturer's website: https://www.agrisera.com/en/artiklar/bak1-bri1-associated-receptor-kinase.html
Anti-BIK1 antibody manufacturer's website: https://www.agrisera.com/en/artiklar/bik1-botrytis-induced-kinase-1.html
Anti-MPK3 antibody manufacturer's website: https://www.sigmaaldrich.com/catalog/product/sigma/m8318
Anti-MPK6 antibody manufacturer's website: https://www.sigmaaldrich.com/catalog/product/sigma/a7104
Anti-Flag antibody manufacturer's website: https://www.sigmaaldrich.com/catalog/product/sigma/f3165
Anti-HA antibody manufacturer's website: http://www.ab-mart.com.cn/page.aspx?node=60&id=963
Goat Anti-Rabbit IgG HRP antibody manufacturer's website: http://www.ab-mart.com.cn/page.aspx?node=62&id=980
Goat Anti-Mouse IgG HRP antibody manufacturer's website: http://www.ab-mart.com.cn/page.aspx?node=62&id=960
Anti-RIN4 antibody was used according to Lee et al., 2015., Plant cell., 27:2042-2056.
Anti-pSer343pSer347 antibody was used according to Li et al., 2014., Cell host microbe., 15:329-38.